

## Development of triangular flat-shell element using a new thin-thick plate bending element based on semiLoof constrains

Yong-Liang Chen<sup>†</sup>, Song Cen<sup>‡</sup> and Zhen-Han Yao<sup>‡†</sup>

*Department of Engineering Mechanics, Tsinghua University, Beijing 100084, China*

Yu-Qiu Long<sup>‡†</sup>

*Department of Civil Engineering, Tsinghua University, Beijing 100084, China*

Zhi-Fei Long<sup>‡†</sup>

*Department of Science & Art, China University of Mining & Technology, Beijing 100083, China*

*(Received April 19, 2002, Accepted November 12, 2002)*

**Abstract.** A new simple 3-node triangular flat-shell element with standard nodal DOF (6 DOF per node) is proposed for the linear and geometrically nonlinear analysis of very thin to thick plate and shell structures. The formulation of element GT9 (Long and Xu 1994), a generalized conforming membrane element with rigid rotational freedoms, is employed as the membrane component of the new shell element. Both one-point reduced integration scheme and a corresponding stabilization matrix are adopted for avoiding membrane locking and hourglass phenomenon. The bending component of the new element comes from a new generalized conforming Kirchhoff-Mindlin plate element TSL-T9, which is derived in this paper based on semiLoof constrains and rational shear interpolation. Thus the convergence can be guaranteed and no shear locking will happen. Furthermore, a simple hybrid procedure is suggested to improve the stress solutions, and the Updated Lagrangian formulae are also established for the geometrically nonlinear problems. Numerical results with solutions, which are solved by some other recent element models and the models in the commercial finite element software ABAQUS, are presented. They show that the proposed element, denoted as GMST18, exhibits excellent and better performance for the analysis of thin-thick plates and shells in both linear and geometrically nonlinear problems.

**Key words:** finite element; flat-shell element; generalized conforming; semiLoof constrains geometrical nonlinear; UL formulation; GMST18.

---

### 1. Introduction

The 3-node triangular flat-shell element is widely used in the analysis of shell structures because

---

<sup>†</sup> PhD Candidate

<sup>‡</sup> PhD, Lecturer

<sup>‡†</sup> Professor

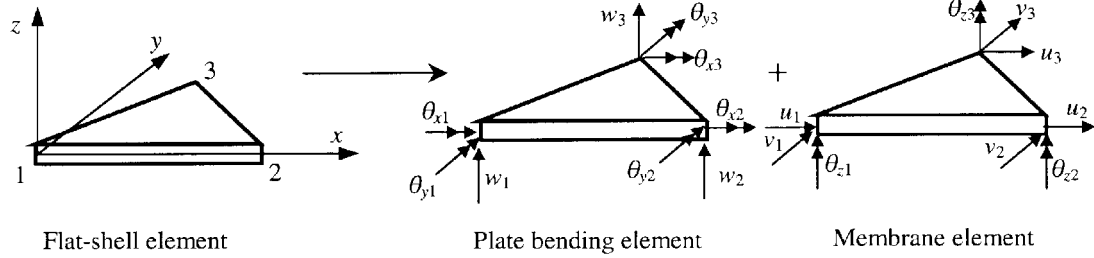
its outstanding merits, such as simplicity, easy application and high accuracy. Therefore, a great deal of attention has been paid to develop an efficient model (Darendeliler, Oral and Turgut 1999, Fish and Belytshko 1992, Providas and Kattis 2000, To and Liu 1994, Wanji and Cheung 1999, Zhang, Lu and Kuang 1998, Zienkiewicz and Taylor 2000).

The formulation of the flat-shell element is composed of two parts: membrane component and plate bending component. The most conventional model is made of the constant strain element CST and the standard nine-DOF plate bending element. But a difficulty arises if all the elements meeting at a node are co-planar: the global stiffness matrix will be singular. This problem can be easily avoided if the membrane element with drilling degrees of freedoms is used (Providas and Kattis 2000). Allman (1984 and 1988), Felippa and Alexander (1992), proposed triangular membrane elements with vertex rotational degrees of freedoms. Long and Xu (1994), also proposed generalized conforming triangular membrane elements with vertex rigid rotational freedoms. Some of these elements have been successfully utilized to construct flat-shell elements (Zhang, Cheung and Chen 2000).

Plate bending element is the other component of the flat-shell element. The development of “thin ( $C^1$ -continuity)” or “thick ( $C^0$ -continuity)” plate elements has attracted many researchers for more than 40 years. Various models have been proposed since 1960s. For thin plate, the non-conforming element BCIZ (Bazeley, Cheung, Irons and Zienkiewicz 1965), the discrete Kirchhoff triangle DKT (Batoz, Bathe and Ho 1980) and their enhanced versions (Cheung and Wanji 1995, Wanji and Cheung 1998) are the most well-known and popular models. Besides, some other high performance elements were also presented by using generalized conforming element method (Long and Zhao 1988, Long and Xin 1989, Long 1993, Long, Bu, Long and Xu 1995). Though these models all exhibit good abilities, they neglect the effects due to transverse shear strains and can only be used in thin plate analysis. Recently, several approaches are applied to generalize thin plate element DKT to Mindlin plate elements (Batoz and Lardeur 1989, Batoz and Katili 1992, Katili 1993, Soh, Long and Cen 1999, Wanji and Cheung 2001). Other  $C^0$ -continuity Mindlin type elements are also successfully constructed at the same time (Ayad, Dhatt and Batoz 1998, Ayad, Rigolot and Talbi 2001, Taylor and Auricchio 1993).

The foregoing efforts provide plentiful choices to develop high performance flat-shell element. The key is how to make a rational selection of membrane and plate elements. From authors' opinions, the new element should include following characters: (1) relative large range for application, i.e., be valid for both thin and thick plates and shells; (2) relative simple formulation without any numerical difficulties and problems, such as singularity of stiffness matrix, shear locking, membrane locking, and hourglass; (3) high accuracy and good convergence for arbitrary mesh division.

In this paper, a new 3-node, 18-DOF triangular flat-shell element is developed. The formulation of the membrane part is modeled by the generalized conforming membrane element, GT9 (Long and Xu 1994), with rigid rotational freedoms. Both one-point reduced integration scheme and a corresponding stabilization matrix (Fish and Belytshko 1992) are adopted for avoiding membrane locking and hourglass phenomenon. The formulation of the bending part is based on a new generalized conforming thin-thick plate element TSL-T9, which is derived in this paper by using semiLoof constrains method (Long 1993) and rational shear interpolation approach (Soh, Long and Cen 1999). Furthermore, a simple hybrid procedure is suggested to improve the stress solutions, and the Updated Lagrangian formulae are also established for the geometrically nonlinear problems. Then the resulting element, called GSMT18, is introduced into the commercial finite element

Fig. 1 Flat-shell element in the local co-ordinate system  $xyz$ 

software ABAQUS (ABAQUS/Standard User's Manual 1998) by user element function and examined by various examples. The numerical results show that present element GSMT18 is free of membrane and shear locking and robust for both thin to thick plates and shells.

## 2. Finite element formulation

Consider the triangular flat-shell element shown in Fig. 1. The element is assembled by plane membrane and plate bending element. It has 3 nodes and 6 DOF per node. The element nodal displacement vector in local coordinate system  $xyz$  is:

$$\mathbf{a}^e = \begin{Bmatrix} \mathbf{a}_1^e \\ \mathbf{a}_2^e \\ \mathbf{a}_3^e \end{Bmatrix} \quad \text{with} \quad \mathbf{a}_i^e = [u_i \ v_i \ w_i \ \theta_{xi} \ \theta_{yi} \ \theta_{zi}]^T \quad (i = 1, 2, 3) \quad (1)$$

where  $u_i$ ,  $v_i$  and  $w_i$  are the nodal displacements along the axes  $x$ ,  $y$  and  $z$ , respectively;  $\theta_{xi}$ ,  $\theta_{yi}$  and  $\theta_{zi}$  are the nodal rotation freedoms.

Let  $\mathbf{a}_m^e$  be the nodal displacement vector related to membrane element; and  $\mathbf{a}_p^e$  be the nodal displacement vector related to plate bending element. Then

$$\mathbf{a}_m^e = \begin{Bmatrix} \mathbf{a}_{m1}^e \\ \mathbf{a}_{m2}^e \\ \mathbf{a}_{m3}^e \end{Bmatrix} \quad \text{with} \quad \mathbf{a}_{mi}^e = \begin{Bmatrix} u_i \\ v_i \\ \theta_{zi} \end{Bmatrix}, \quad \mathbf{a}_p^e = \begin{Bmatrix} \mathbf{a}_{p1}^e \\ \mathbf{a}_{p2}^e \\ \mathbf{a}_{p3}^e \end{Bmatrix} \quad \text{with} \quad \mathbf{a}_{pi}^e = \begin{Bmatrix} w_i \\ \theta_{xi} \\ \theta_{yi} \end{Bmatrix} \quad (i = 1, 2, 3) \quad (2)$$

### 2.1 The formulation and the stabilization of the plane membrane element GT9 (Long and Xu 1994)

The membrane element used here is the 3-node triangular generalized conforming membrane element GT9 (Long and Xu 1994) with rigid rotational freedoms, and its displacement field is given by

$$\begin{Bmatrix} u \\ v \end{Bmatrix} = \sum_{i=1}^3 \begin{bmatrix} L_i & 0 & N_{u\theta_i} \\ 0 & L_i & N_{v\theta_i} \end{bmatrix} \mathbf{a}_{mi}^e \quad (3)$$

where  $L_i$  ( $i = 1, 2, 3$ ) are the triangular area coordinates;  $N_{u\theta_i}$  and  $N_{v\theta_i}$  are the shape functions for the

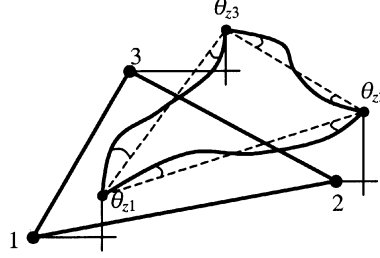


Fig. 2 The additional rigid rotational freedom for membrane element

rigid rotation freedoms  $\theta_{zi}$  (Fig. 2):

$$N_{u\theta_i} = \frac{1}{2}L_i(b_kL_j - b_jL_k), \quad N_{v\theta_i} = \frac{1}{2}L_i(c_kL_j - c_jL_k) \quad (i, j, k = \overleftarrow{1, 2, 3}) \quad (4)$$

with

$$b_i = y_j - y_m, \quad c_i = x_j - x_m \quad (5)$$

Differentiation of Eq. (3) yields the strain matrix of element:

$$\mathbf{B}_m = [\mathbf{B}_{m1} \quad \mathbf{B}_{m2} \quad \mathbf{B}_{m3}] \quad (6)$$

where

$$\mathbf{B}_{mi} = \frac{1}{4A} \begin{bmatrix} 2b_i & 0 & b_i(b_kL_j - b_jL_k) \\ 0 & 2c_i & c_i(c_kL_j - c_jL_k) \\ 2c_i & 2b_i & (b_ic_k + b_kc_i)L_j - (b_ic_j + b_jc_i)L_k \end{bmatrix}, \quad (i, j, k = \overleftarrow{1, 2, 3}) \quad (7)$$

where  $A$  denotes the area of the element.

Then, the element stiffness matrix of GT9 in the local coordinate system can be obtained as follows:

$$\mathbf{K}_m^e = \iint_{A^e} \mathbf{B}_m^T \mathbf{D}_m \mathbf{B}_m dA \quad (8)$$

where  $\mathbf{D}_m$  is the elasticity matrix:

$$\mathbf{D}_m = \frac{Eh}{1-\nu^2} \begin{bmatrix} 1 & \nu & 0 \\ \nu & 1 & 0 \\ 0 & 0 & \frac{1-\nu}{2} \end{bmatrix} \quad (9)$$

where  $E$  is Young's modulus;  $\nu$  is Poisson's ratio; and  $h$  is the thickness of element.

If  $\theta_{z1} = \theta_{z2} = \theta_{z3}$ , there exists an extra zero energy mode in addition to the conventional rigid body movement. This extra zero energy mode can be easily suppressed by setting one of the nodal rotational to be zero in one element of the mesh (Long and Xu 1994).

In order to avoid membrane locking in the calculation of shells, one-point reduced integration are often employed for the membrane component with rotational freedoms. But unfortunately, extra zero energy modes of the element will appear and hourglass phenomenon may occur. Fish and Belytschko (1992), suggested a method of adding a stabilization matrix to overcome this shortcoming. According

to their approach, the stabilization matrix of the element GT9 is given as follows

$$\mathbf{K}_{mstab}^e = \bar{\omega} \begin{bmatrix} 0 & 0 & 0 & 0 & 0 & 0 & 0 & 0 \\ 0 & 0 & 0 & 0 & 0 & 0 & 0 & 0 \\ 0 & 0 & 2 & 0 & 0 & -1 & 0 & 0 & -1 \\ 0 & 0 & 0 & 0 & 0 & 0 & 0 & 0 & 0 \\ 0 & 0 & 0 & 0 & 0 & 0 & 0 & 0 & 0 \\ 0 & 0 & -1 & 0 & 0 & 2 & 0 & 0 & -1 \\ 0 & 0 & 0 & 0 & 0 & 0 & 0 & 0 & 0 \\ 0 & 0 & 0 & 0 & 0 & 0 & 0 & 0 & 0 \\ 0 & 0 & -1 & 0 & 0 & -1 & 0 & 0 & 2 \end{bmatrix} \quad (10)$$

with

$$\bar{\omega} = \chi[\mathbf{K}_m^{1^e}(3, 3) + \mathbf{K}_m^{1^e}(6, 6) + \mathbf{K}_m^{1^e}(9, 9)]/3 \quad (11)$$

where  $\mathbf{K}_m^{1^e}$  denotes the element stiffness matrix of GT9 using one-point integration;  $\chi$  is a perturbation factor. From numerical experiments, it is found that when  $\chi$  is not less than  $10^{-6}$ , the rank and eigenvalues of the new shell element are correct. So  $\chi = 10^{-6}$  is adopted throughout this paper.

Thus the element stiffness matrix of GT9 in local coordinate system can be modified as

$$\mathbf{K}_m^e = \mathbf{K}_m^{1^e} + \mathbf{K}_{mstab}^e \quad (12)$$

## 2.2 The formulation of the new thin-thick plate bending element TSL-T9

Long (1993), proposed a 9-DOF generalized conforming thin plate element LSL-T9 based on semiLoof constrains. Soh, Long and Cen (1999), proposed a method of assuming shear strain field and extend thin plate element DKT to another thin-thick plate element ARS-T9. Both techniques described in foregoing references are used in this section to construct a new thin-thick plate element TSL-T9: (1) the shear strain field is determined by using Timoshenko's beam theory; (2) the deflection field is assumed and then determined by using semiLoof constrains. Then all the formulae can be obtained following the standard procedure.

Consider the thick plate triangular element shown in Fig. 3, the element nodal displacement vector is:

$$\mathbf{q}^e = [w_1 \ \beta_{x1} \ \beta_{y1} \ w_2 \ \beta_{x2} \ \beta_{y2} \ w_3 \ \beta_{x3} \ \beta_{y3}]^T \quad (13)$$

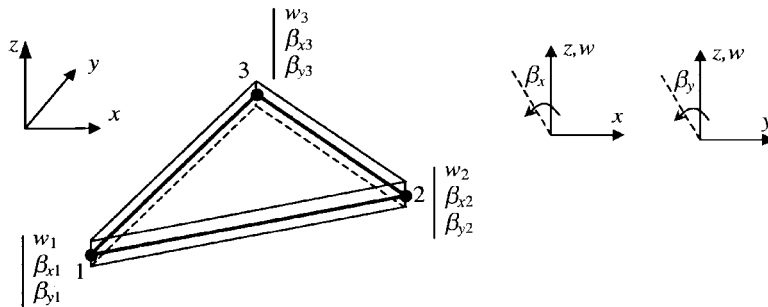


Fig. 3 Triangular plate bending element TSL-T9

The  $\mathbf{q}^e$  and  $\mathbf{a}_p^e$  in Eq. (2) have following relationship:

$$\mathbf{q}^e = \mathbf{L}\mathbf{a}_p^e \text{ with } \mathbf{L} = \begin{bmatrix} \mathbf{I} & \mathbf{0} & \mathbf{0} \\ \mathbf{0} & \mathbf{I} & \mathbf{0} \\ \mathbf{0} & \mathbf{0} & \mathbf{I} \end{bmatrix}, \quad \mathbf{I} = \begin{bmatrix} 1 & 0 & 0 \\ 0 & 0 & -1 \\ 0 & 1 & 0 \end{bmatrix}, \text{ and } \mathbf{0} = \begin{bmatrix} 0 & 0 & 0 \\ 0 & 0 & 0 \\ 0 & 0 & 0 \end{bmatrix} \quad (14)$$

### 2.2.1 Locking-free Timoshenko's beam element

In order to determine the displacements and the shear strain along each element side, a locking-free Timoshenko's beam element was derived and presented by Soh, Long and Cen (1999) and Soh, Cen, Long and Long (2001). The formulas of deflection  $w$ , rotation  $\beta_s$  and shear strain  $\gamma$  for the thick beam element, as shown in Fig. 4, are as follows:

$$w = w_i(1-r) + w_j r + \frac{d}{2}(\beta_{si} - \beta_{sj})r(1-r) - \frac{d}{2}\Gamma(1-2\delta) \cdot r(1-r)(1-2r) \quad (15a)$$

$$\beta_s = \beta_{si}(1-r) + \beta_{sj}r + 3\Gamma(1-2\delta) \cdot r(1-r) \quad (15b)$$

$$\gamma = \frac{1}{d}\frac{\partial w}{\partial r} - \beta_s = \delta\Gamma \quad (15c)$$

with

$$\Gamma = \frac{2}{d}(-w_i + w_j) - \beta_{si} - \beta_{sj}, \quad \delta = \frac{6\lambda}{1+12\lambda}, \quad \lambda = \frac{D_d}{C_d d^2} \quad (16)$$

where  $d$  is the length of the beam.  $D_d$  and  $C_d$  are the bending and shear stiffness of the beam, respectively. Since the deflection, rotation and shear strain along the sides of the plate element will be given by Eqs. (15) and (16),  $D_d$  and  $C_d$  should be replaced by the corresponding quantities of the plate. So the parameter  $\delta$  in Eqs. (15) and (16) can be rewritten as:

$$\delta = \frac{\left(\frac{h}{d}\right)^2}{\frac{5}{6}(1-\nu) + 2\left(\frac{h}{d}\right)^2} \quad (17)$$

where  $h$  is the thickness of the element;  $\nu$  is Poisson's ratio.

It can be seen that when the thickness  $h$  approaches zero, the shear strain  $\gamma$  will vanish automatically, and no shear locking will happen.

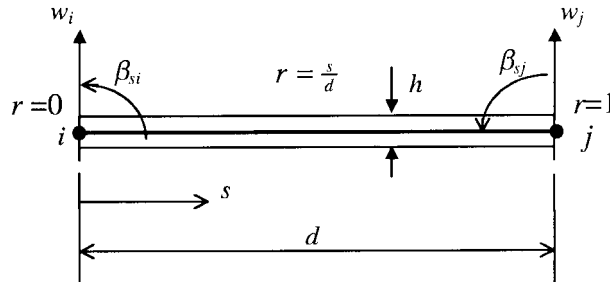


Fig. 4 The Timoshenko's beam element

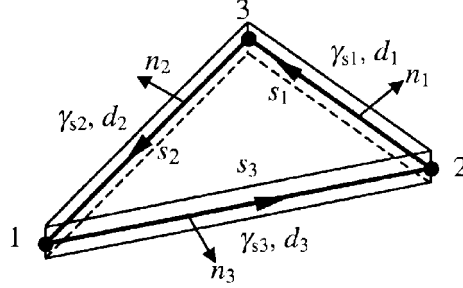


Fig. 5 The shear strain  $\gamma_{s_i}$ , length  $d_i$ , normal and tangential direction ( $n_i, s_i$ ) of each element side

### 2.2.2 Interpolation formulas for the shear strain fields

The interpolation procedure for transverse shear strain fields is the same as that of Soh, Long and Cen (1999). As shown in Fig. 5, the shear strain along the tangential direction of each element side is constant and determined by Timoshenko's beam formulae (15c). And from some simple geometrical relations, the shear strain fields can be obtained as follows:

$$\boldsymbol{\gamma} = \begin{Bmatrix} \gamma_{xz} \\ \gamma_{yz} \end{Bmatrix} = \mathbf{H}\Delta\mathbf{G}\mathbf{q}^e = \mathbf{B}_s\mathbf{a}_p^e \quad (18)$$

where  $\mathbf{B}_s$  is the shear strain matrix;

$$\mathbf{B}_s = \mathbf{H}\Delta\mathbf{G}\mathbf{L} \quad (19)$$

with

$$\mathbf{H} = \frac{1}{2A} \begin{bmatrix} b_3L_2 & -b_2L_3 & b_1L_3 & -b_3L_1 & b_2L_1 & -b_1L_2 \\ c_3L_2 & -c_2L_3 & c_1L_3 & -c_3L_1 & c_2L_1 & -c_1L_2 \end{bmatrix} \quad (20)$$

$$\Delta = \begin{bmatrix} \delta_1 & 0 & 0 \\ 0 & \delta_2 & 0 \\ 0 & 0 & \delta_3 \end{bmatrix} \quad \text{with} \quad \delta_i = \frac{\left(\frac{h}{d_i}\right)^2}{\frac{5}{6}(1-\nu) + 2\left(\frac{h}{d_i}\right)^2} \quad (i = 1, 2, 3) \quad (21)$$

$$\mathbf{G} = \begin{bmatrix} 0 & 0 & 0 & -2 & -c_1 & b_1 & 2 & c_1 & b_1 \\ 2 & -c_2 & b_2 & 0 & 0 & 0 & -2 & -c_2 & b_2 \\ -2 & -c_3 & b_3 & 2 & -c_3 & b_3 & 0 & 0 & 0 \end{bmatrix} \quad (22)$$

where  $b_i$  and  $c_i$  ( $i = 1, 2, 3$ ) are given in (5);  $d_i$  is the length of the  $i$ th element side (Fig. 5). It is obvious that when  $h \rightarrow 0$ ,  $\Delta \rightarrow \mathbf{0}$ , and  $\boldsymbol{\gamma} \rightarrow 0$ .

### 2.2.3 Interpolation formulas for the deflection field

According to Long (1993), the element deflection field  $w$  is assumed to be a polynomial with 12 terms:

$$w = \mathbf{F}_\lambda \boldsymbol{\lambda} \quad (23)$$

with

$$\boldsymbol{\lambda} = [\lambda_1 \ \lambda_2 \ \lambda_3 \ \lambda_4 \ \lambda_5 \ \lambda_6 \ \lambda_7 \ \lambda_8 \ \lambda_9 \ \lambda_{10} \ \lambda_{11} \ \lambda_{12}]^T \quad (24)$$

$$\mathbf{F}_\lambda = [L_1 \ L_2 \ L_3 \ L_2L_3 \ L_3L_1 \ L_1L_2 \ L_2L_3(L_2-L_3) \ L_3L_1(L_3-L_1) \ L_1L_2(L_1-L_2) \\ L_1^2L_2L_3 \ L_2^2L_3L_1 \ L_3^2L_1L_2] \quad (25)$$

### 2.2.4 The rotation field

Based on the Mindlin plate theory, the rotation field can be obtained:

$$\boldsymbol{\beta} = \begin{Bmatrix} \beta_x \\ \beta_y \end{Bmatrix} = \begin{Bmatrix} \frac{\partial w}{\partial x} - \gamma_{xz} \\ \frac{\partial w}{\partial y} - \gamma_{yz} \end{Bmatrix} = \begin{bmatrix} \mathbf{F}_{\lambda,x} \\ \mathbf{F}_{\lambda,y} \end{bmatrix} \boldsymbol{\lambda} - \mathbf{H}\Delta \mathbf{G} \mathbf{q}^e \quad (26)$$

where  $(, x)$  and  $(, y)$  mean the derivatives respect to  $x$  and  $y$ , and

$$\frac{\partial}{\partial x} = \frac{1}{2A} \left( b_1 \frac{\partial}{\partial L_1} + b_2 \frac{\partial}{\partial L_2} + b_3 \frac{\partial}{\partial L_3} \right) \\ \frac{\partial}{\partial y} = \frac{1}{2A} \left( c_1 \frac{\partial}{\partial L_1} + c_2 \frac{\partial}{\partial L_2} + c_3 \frac{\partial}{\partial L_3} \right) \quad (27)$$

### 2.2.5 The deflections and normal slopes along element sides

Along each side of the element, the deflection  $\tilde{w}$  is determined by Eq. (15a); and the normal slope  $\tilde{\beta}_n$  is assumed to distribute linearly. For example, the deflection and normal slope along side 23 are as follows

$$\tilde{w}_{23} = [L_2 + \mu_{e1}L_2L_3(L_2-L_3)]w_2 + \frac{1}{2}L_2L_3[1 + \mu_{e1}(L_2-L_3)](c_1\beta_{x2} - b_1\beta_{y2}) \\ + [L_3 - \mu_{e1}L_2L_3(L_2-L_3)]w_3 + \frac{1}{2}L_2L_3[-1 + \mu_{e1}(L_2-L_3)](c_1\beta_{x3} - b_1\beta_{y3}) \quad (28a)$$

$$\tilde{\beta}_{n23} = -\frac{L_2}{d_1}(b_1\beta_{x2} + c_1\beta_{y2}) - \frac{L_3}{d_1}(b_1\beta_{x3} + c_1\beta_{y3}) \quad (28b)$$

with

$$\mu_{ei} = 1 - 2\delta_i \quad (i = 1, 2, 3) \quad (29)$$

### 2.2.6 The semiLoof constrains

In order to solve  $\boldsymbol{\lambda}$  in term of  $\mathbf{q}^e$ , 12 semiLoof point compatibility conditions (Fig. 6) are established (Long 1993).

First, apply the compatibility conditions for deflections at the corner nodes 1, 2, 3

$$(w - \tilde{w})_i = 0 \quad (i = 1, 2, 3) \quad (30)$$

$\lambda_1, \lambda_2, \lambda_3$  can be solved

$$\lambda_1 = w_1, \quad \lambda_2 = w_2, \quad \lambda_3 = w_3 \quad (31)$$

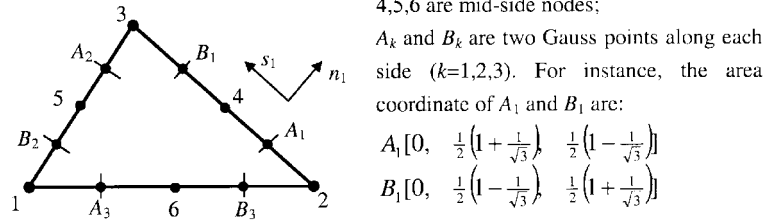


Fig. 6 SemiLoof constrain points

Then, apply the compatibility conditions for deflections at the mid-side points 4, 5, 6

$$(w - \tilde{w})_j = 0 \quad (j = 4, 5, 6) \quad (32)$$

$\lambda_4, \lambda_5, \lambda_6$  can be solved

$$\lambda_4 = \frac{c_1}{2}(\beta_{x2} - \beta_{x3}) - \frac{b_1}{2}(\beta_{y2} - \beta_{y3})$$

$$\lambda_5 = \frac{c_2}{2}(\beta_{x3} - \beta_{x1}) - \frac{b_2}{2}(\beta_{y3} - \beta_{y1})$$

$$\lambda_6 = \frac{c_3}{2}(\beta_{x1} - \beta_{x2}) - \frac{b_3}{2}(\beta_{y1} - \beta_{y2}) \quad (33)$$

Finally, apply the compatibility conditions for normal slopes at Gauss points A and B along each side

$$(\beta_n - \tilde{\beta}_n)_k = 0 \quad (k = A_1, B_1, A_2, B_2, A_3, B_3) \quad (34)$$

where  $\beta_n$  is derived from Eq. (26). And for example, along side  $\bar{23}$

$$\beta_{n23} = -\frac{b_1}{d_1}\beta_x \Big|_{L_1=0} - \frac{c_1}{d_1}\beta_y \Big|_{L_1=0} \quad (35)$$

Substituting Eqs. (35) and (28b) into Eq. (34),  $\lambda_7, \dots, \lambda_{12}$  can be solved. In this solution, the last three coefficients are equal, i.e.,  $\lambda_{10} = \lambda_{11} = \lambda_{12}$ . Therefore, the element deflection field can be rewritten in term of 10 coefficients

$$w = \mathbf{F}'_{\lambda} \boldsymbol{\lambda}' \quad (36)$$

where

$$\boldsymbol{\lambda}' = [\lambda_1 \ \lambda_2 \ \lambda_3 \ \lambda_4 \ \lambda_5 \ \lambda_6 \ \lambda_7 \ \lambda_8 \ \lambda_9 \ \lambda_{10}]^T \quad (37)$$

$$\mathbf{F}'_{\lambda} = [L_1 \ L_2 \ L_3 \ L_2L_3 \ L_3L_1 \ L_1L_2 \ L_2L_3(L_2 - L_3) \ L_3L_1(L_3 - L_1) \\ L_1L_2(L_1 - L_2) \ L_1L_2L_3] \quad (38)$$

Combining the above results,  $\boldsymbol{\lambda}'$  can be expressed in terms of  $\mathbf{q}^e$  as follows:

$$\boldsymbol{\lambda}' = \mathbf{C}\mathbf{q}^e \quad (39)$$

where

$$\mathbf{C} = [\mathbf{C}_1 \ \mathbf{C}_2 \ \mathbf{C}_3] \quad (40)$$

$C_1 =$ 

$$\begin{bmatrix}
1 & 0 & 0 \\
0 & 0 & 0 \\
0 & 0 & 0 \\
0 & 0 & 0 \\
0 & -\frac{1}{2}c_2 & \frac{1}{2}b_2 \\
0 & \frac{1}{2}c_3 & -\frac{1}{2}b_3 \\
\frac{1}{2}(r_2+r_3)-\left(\frac{1}{3}+r_2\right)\delta_2 & \frac{1}{12}(c_1-3r_2c_2+3r_3c_3)+\frac{1}{6}(1+3r_2)c_2\delta_2 & -\frac{1}{12}(b_1-3r_2b_2+3r_3b_3)-\frac{1}{6}(1+3r_2)b_2\delta_2 \\
+\left(\frac{1}{3}-r_3\right)\delta_3 & +\frac{1}{6}(1-3r_3)c_3\delta_3 & -\frac{1}{6}(1-3r_3)b_3\delta_3 \\
-\frac{1}{2}(3+r_3)+\frac{8}{3}\delta_2 & -\frac{1}{12}(3r_3c_3+c_3-8c_2)-\frac{4}{3}c_2\delta_2 & \frac{1}{12}(3r_3b_3+b_3-8b_2)+\frac{4}{3}b_2\delta_2 \\
+\left(\frac{1}{3}+r_3\right)\delta_3 & +\frac{1}{6}(1+3r_3)c_3\delta_3 & -\frac{1}{6}(1+3r_3)b_3\delta_3 \\
\frac{1}{2}(3-r_2)-\left(\frac{1}{3}-r_2\right)\delta_2 & \frac{1}{12}(3r_2c_2-c_2+8c_3)+\frac{1}{6}(1-3r_2)c_2\delta_2 & -\frac{1}{12}(3r_2b_2-b_2+8b_3)-\frac{1}{6}(1-3r_2)b_2\delta_2 \\
-\frac{8}{3}\delta_3 & -\frac{4}{3}c_3\delta_3 & +\frac{4}{3}b_3\delta_3 \\
(r_3-r_2)+2(r_2\delta_2-r_3\delta_3) & \frac{1}{2}(r_2c_2+r_3c_3)-r_2c_2\delta_2-r_3c_3\delta_3 & -\frac{1}{2}(r_2b_2+r_3b_3)+r_2b_2\delta_2+r_3b_3\delta_3
\end{bmatrix} \quad (41a)$$

 $C_2 =$ 

$$\begin{bmatrix}
0 & 0 & 0 \\
1 & 0 & 0 \\
0 & 0 & 0 \\
0 & \frac{1}{2}c_1 & -\frac{1}{2}b_1 \\
0 & 0 & 0 \\
0 & -\frac{1}{2}c_3 & \frac{1}{2}b_3 \\
\frac{1}{2}(3-r_3)-\left(\frac{1}{3}-r_3\right)\delta_3 & \frac{1}{12}(3r_3c_3-c_3+8c_1)+\frac{1}{6}(1-3r_3)c_3\delta_3 & -\frac{1}{12}(3r_3b_3-b_3+8b_1)-\frac{1}{6}(1-3r_3)b_3\delta_3 \\
-\frac{8}{3}\delta_1 & -\frac{4}{3}c_1\delta_1 & +\frac{4}{3}b_1\delta_1 \\
\frac{1}{2}(r_3+r_1)-\left(\frac{1}{3}+r_3\right)\delta_3 & \frac{1}{12}(c_2-3r_3c_3+3r_1c_1)+\frac{1}{6}(1+3r_3)c_3\delta_3 & -\frac{1}{12}(b_2-3r_3b_3+3r_1b_1)-\frac{1}{6}(1+3r_3)b_3\delta_3 \\
+\left(\frac{1}{3}-r_1\right)\delta_1 & +\frac{1}{6}(1-3r_1)c_1\delta_1 & -\frac{1}{6}(1-3r_1)b_1\delta_1 \\
-\frac{1}{2}(3+r_1)+\frac{8}{3}\delta_3 & -\frac{1}{12}(3r_1c_1+c_1-8c_3)-\frac{4}{3}c_3\delta_3 & \frac{1}{12}(3r_1b_1+b_1-8b_3)+\frac{4}{3}b_3\delta_3 \\
+\left(\frac{1}{3}+r_1\right)\delta_1 & +\frac{1}{6}(1+3r_1)c_1\delta_1 & -\frac{1}{6}(1+3r_1)b_1\delta_1 \\
(r_1-r_3)+2(r_3\delta_3-r_1\delta_1) & \frac{1}{2}(r_3c_3+r_1c_1)-r_3c_3\delta_3-r_1c_1\delta_1 & -\frac{1}{2}(r_3b_3+r_1b_1)+r_3b_3\delta_3+r_1b_1\delta_1
\end{bmatrix} \quad (41b)$$

$$\mathbf{C}_3 = \begin{bmatrix} 0 & 0 & 0 \\ 0 & 0 & 0 \\ 1 & 0 & 0 \\ 0 & -\frac{1}{2}c_1 & \frac{1}{2}b_1 \\ 0 & \frac{1}{2}c_2 & -\frac{1}{2}b_2 \\ -\frac{1}{2}(3+r_2)+\frac{8}{3}\delta_1 & -\frac{1}{12}(3r_2c_2+c_2-8c_1)-\frac{4}{3}c_1\delta_1 & \frac{1}{12}(3r_2b_2+b_2-8b_1)+\frac{4}{3}b_1\delta_1 \\ +\left(\frac{1}{3}+r_2\right)\delta_2 & +\frac{1}{6}(1+3r_2)c_2\delta_2 & -\frac{1}{6}(1+3r_2)b_2\delta_2 \\ \frac{1}{2}(3-r_1)-\left(\frac{1}{3}-r_1\right)\delta_1 & \frac{1}{12}(3r_1c_1-c_1+8c_2)+\frac{1}{6}(1-3r_1)c_1\delta_1 & -\frac{1}{12}(3r_1b_1-b_1+8b_2)-\frac{1}{6}(1-3r_1)b_1\delta_1 \\ -\frac{8}{3}\delta_2 & -\frac{4}{3}c_2\delta_2 & +\frac{4}{3}b_2\delta_2 \\ \frac{1}{2}(r_1+r_2)-\left(\frac{1}{3}+r_1\right)\delta_1 & \frac{1}{12}(c_3-3r_1c_1+3r_2c_2)+\frac{1}{6}(1+3r_1)c_1\delta_1 & -\frac{1}{12}(b_3-3r_1b_1+3r_2b_2)-\frac{1}{6}(1+3r_1)b_1\delta_1 \\ +\left(\frac{1}{3}-r_2\right)\delta_2 & +\frac{1}{6}(1-3r_2)c_2\delta_2 & -\frac{1}{6}(1-3r_2)b_2\delta_2 \\ (r_2-r_1)+2(r_1\delta_1-r_2\delta_2) & \frac{1}{2}(r_1c_1+r_2c_2)-r_1c_1\delta_1-r_2c_2\delta_2 & -\frac{1}{2}(r_1b_1+r_2b_2)+r_1b_1\delta_1+r_2b_2\delta_2 \end{bmatrix} \quad (41c)$$

where

$$r_1 = \frac{d_2^2 - d_3^2}{d_1^2}, \quad r_2 = \frac{d_3^2 - d_1^2}{d_2^2}, \quad r_3 = \frac{d_1^2 - d_2^2}{d_3^2} \quad (42)$$

Substituting Eq. (39) into Eq. (36),  $w$  can be expressed as

$$w = \mathbf{F}'_{\lambda} \mathbf{C} \mathbf{q}^e = \mathbf{F}'_{\lambda} \mathbf{C} \mathbf{L} \mathbf{a}_p^e = \mathbf{N}^e \mathbf{a}_p^e \quad \text{with} \quad \mathbf{N}^e = \mathbf{F}'_{\lambda} \mathbf{C} \mathbf{L} \quad (43)$$

where  $\mathbf{N}^e$  is the shape function matrix for the deflection field  $w$ . As the statement in (Long 1993), the deflection field  $w$  and the rotation field  $\boldsymbol{\beta}$  are not exactly compatible with the deflection and rotation along the element sides. But it satisfies following relaxed compatible conditions (Long 1992):

$$\oint_{\partial A^e} [T_n(w - \tilde{w}) - M_n(\boldsymbol{\beta}_n - \tilde{\boldsymbol{\beta}}_n) - M_{ns}(\boldsymbol{\beta}_s - \tilde{\boldsymbol{\beta}}_s)] = 0 \quad (44)$$

where  $T_n$ ,  $M_n$  and  $M_{ns}$  are the boundary shear force, normal moment and tangential moment on element boundary  $\partial A^e$ . Thus, from the concept of generalized conforming (Long and Zhao 1988, Long and Xin 1989, Long 1992, Long 1993, Long, Bu, Long and Xu 1995), the element presented here is also a generalized conforming element, and the convergence can be guaranteed.

### 2.2.7 The stiffness matrix for plate bending element

From Eqs. (26), (36) and (39), the rotation field  $\boldsymbol{\beta}$  can be rewritten as

$$\boldsymbol{\beta} = \begin{Bmatrix} \beta_x \\ \beta_y \end{Bmatrix} = \begin{Bmatrix} \frac{\partial w}{\partial x} - \gamma_{xz} \\ \frac{\partial w}{\partial y} - \gamma_{yz} \end{Bmatrix} = \left( \begin{bmatrix} \mathbf{F}'_{\lambda, x} \\ \mathbf{F}'_{\lambda, y} \end{bmatrix} \mathbf{C} - \mathbf{H} \Delta \mathbf{G} \right) \mathbf{L} \mathbf{a}_p^e \quad (45)$$

Then, the curvature field  $\boldsymbol{\kappa}$  of the bending element is

$$\boldsymbol{\kappa} = \begin{Bmatrix} \kappa_x \\ \kappa_y \\ 2\kappa_{xy} \end{Bmatrix} = \begin{Bmatrix} -\frac{\partial\beta_x}{\partial x} \\ -\frac{\partial\beta_y}{\partial y} \\ -\frac{\partial\beta_x}{\partial y} - \frac{\partial\beta_y}{\partial x} \end{Bmatrix} = \left( - \begin{bmatrix} F'_{\lambda,xx} \\ F'_{\lambda,yy} \\ F'_{\lambda,xy} \end{bmatrix} \mathbf{CL} \right) \mathbf{a}_p^e = \mathbf{B}_b \mathbf{a}_p^e \quad (46)$$

where  $\mathbf{B}_b$  is the bending strain matrix, and

$$\begin{aligned} F'_{\lambda,xx} &= \frac{1}{2A^2} [0 \ 0 \ 0 \ b_2b_3 \ b_3b_1 \ b_1b_2 \\ &\quad b_2^2L_3 - b_3^2L_2 + 2b_2b_3(L_2 - L_3) \ b_3^2L_1 - b_1^2L_3 + 2b_3b_1(L_3 - L_1) \ b_1^2L_2 - b_2^2L_1 + 2b_1b_2(L_1 - L_2) \\ &\quad b_2b_3L_1 + b_3b_1L_2 + b_1b_2L_3] \end{aligned} \quad (47a)$$

$$\begin{aligned} F'_{\lambda,yy} &= \frac{1}{2A^2} [0 \ 0 \ 0 \ c_2c_3 \ c_3c_1 \ c_1c_2 \\ &\quad c_2^2L_3 - c_3^2L_2 + 2c_2c_3(L_2 - L_3) \ c_3^2L_1 - c_1^2L_3 + 2c_3c_1(L_3 - L_1) \ c_1^2L_2 - c_2^2L_1 + 2c_1c_2(L_1 - L_2) \\ &\quad c_2c_3L_1 + c_3c_1L_2 + c_1c_2L_3] \end{aligned} \quad (47b)$$

$$\begin{aligned} F'_{\lambda,xy} &= \frac{1}{4A^2} [0 \ 0 \ 0 \ b_2c_3 + b_3c_2 \ b_3c_1 + b_1c_3 \ b_1c_2 + b_2c_1 \\ &\quad 2(b_2c_3 + b_3c_2 - b_3c_3)L_2 + 2(b_2c_2 - b_2c_3 - b_3c_2)L_3 \ 2(b_3c_1 + b_1c_3 - b_1c_1)L_3 + 2(b_3c_3 - b_3c_1 - b_1c_3)L_1 \\ &\quad 2(b_1c_2 + b_2c_1 - b_2c_2)L_1 + 2(b_1c_1 - b_1c_2 - b_2c_1)L_2 \ (b_2c_3 + b_3c_2)L_1 + (b_3c_1 + b_1c_3)L_2 + (b_1c_2 + b_2c_1)L_3] \end{aligned} \quad (47c)$$

Thus, the stiffness matrix for the plate bending element can be obtained

$$\mathbf{K}_p^e = \iint_{A^e} \mathbf{B}_b^T \mathbf{D}_b \mathbf{B}_b dA + \iint_{A^e} \mathbf{B}_s^T \mathbf{D}_s \mathbf{B}_s dA \quad (48)$$

where

$$\mathbf{D}_b = D \begin{bmatrix} 1 & \nu & 0 \\ \nu & 1 & 0 \\ 0 & 0 & \frac{1-\nu}{2} \end{bmatrix} = \frac{Eh^2}{12(1-\nu^2)} \begin{bmatrix} 1 & \nu & 0 \\ \nu & 1 & 0 \\ 0 & 0 & \frac{1-\nu}{2} \end{bmatrix}, \quad \mathbf{D}_s = \frac{5}{6} Gh \begin{bmatrix} 1 & 0 \\ 0 & 1 \end{bmatrix} \quad (49)$$

where  $G = E/[2(1-\nu)]$  is the shear modulus. A standard 3 Hammer integration point scheme is employed in executing Eq. (48) in order to satisfy the theoretical necessity. It is not necessary to use any reduced integration techniques here.

This plate bending element obtained is named TSL-T9, to remind that it is a Thick plate

SemiLoof Triangular finite element with 9 DOFs. It can degenerate into the generalized conforming thin plate element LSL-T9 presented by (Long 1993) when let the parameters  $\delta_i (i = 1, 2, 3)$  equal zero. So TSL-T9 is a Kirchhoff-Mindlin element.

### 2.2.8 Hybrid-enhanced procedure for stress solutions

From the constitutive relations of the plate, the bending moments and shear forces can be obtained.

$$\mathbf{M} = \begin{Bmatrix} M_x \\ M_y \\ M_{xy} \end{Bmatrix} = \mathbf{D}_b \boldsymbol{\kappa} = \mathbf{D}_b \mathbf{B}_b \mathbf{a}_p^e, \quad \mathbf{T} = \begin{Bmatrix} T_x \\ T_y \end{Bmatrix} = \mathbf{D}_s \boldsymbol{\gamma} = \mathbf{D}_s \mathbf{B}_s \mathbf{a}_p^e \quad (50)$$

It is a well-known fact that hybrid elements are likely to perform better than displacement elements for calculation of stresses. In order to improve the stress solutions of the presented element, a simple hybrid-enhanced procedure is suggested here.

The bending moment field  $\mathbf{M}$  and the shear force field  $\mathbf{T}$  are only required to satisfy  $C^{-1}$ -continuity between two elements based on Mindlin plate theory (Ayad, Dhatt and Batoz 1998, Ayad, Rigolot, Talbi 2001). Thus,  $\mathbf{M}$  can be assumed as follows:

$$\mathbf{M} = \mathbf{P}_M \boldsymbol{\alpha}_M \quad (51)$$

where

$$\mathbf{P}_M = \begin{bmatrix} L_1 & L_2 & L_3 & 0 & 0 & 0 & 0 & 0 & 0 \\ 0 & 0 & 0 & L_1 & L_2 & L_3 & 0 & 0 & 0 \\ 0 & 0 & 0 & 0 & 0 & 0 & L_1 & L_2 & L_3 \end{bmatrix} \quad (52)$$

$$\boldsymbol{\alpha}_M = [\alpha_1 \ \alpha_2 \ \alpha_3 \ \alpha_4 \ \alpha_5 \ \alpha_6 \ \alpha_7 \ \alpha_8 \ \alpha_9]^T \quad (53)$$

$\alpha_i (i = 1, 2, \dots, 9)$  are 9 unknown parameters.

From the equilibrium equations of a plate, the shear force field  $\mathbf{T}$  can be expressed as:

$$\mathbf{T} = \begin{Bmatrix} T_x \\ T_y \end{Bmatrix} = \begin{Bmatrix} M_{x,x} + M_{xy,y} \\ M_{xy,x} + M_{y,y} \end{Bmatrix} = \mathbf{P}_T \boldsymbol{\alpha}_M \quad (54)$$

where

$$\mathbf{P}_T = \frac{1}{2A} \begin{bmatrix} b_1 & b_2 & b_3 & 0 & 0 & 0 & c_1 & c_2 & c_3 \\ 0 & 0 & 0 & c_1 & c_2 & c_3 & b_1 & b_2 & b_3 \end{bmatrix} \quad (55)$$

By employing Hellinger-Reissner variational principle, the energy functional of the plate element can be expressed as:

$$\begin{aligned} \Pi_R^e &= -\frac{1}{2} \iint_{A^e} \mathbf{M}^T \mathbf{D}_b^{-1} \mathbf{M} dA - \frac{1}{2} \iint_{A^e} \mathbf{T}^T \mathbf{D}_s^{-1} \mathbf{T} dA + \iint_{A^e} \mathbf{M}^T \boldsymbol{\kappa} dA + \iint_{A^e} \mathbf{T}^T \boldsymbol{\gamma} dA - W_{\text{exp}} \\ &= -\frac{1}{2} \boldsymbol{\alpha}_M^T \left[ \iint_{A^e} (\mathbf{P}_M^T \mathbf{D}_b^{-1} \mathbf{P}_M + \mathbf{P}_T^T \mathbf{D}_s^{-1} \mathbf{P}_T) dA \right] \boldsymbol{\alpha}_M + \boldsymbol{\alpha}_M^T \left[ \iint_{A^e} (\mathbf{P}_M^T \mathbf{B}_b + \mathbf{P}_T^T \mathbf{B}_s) dA \right] \mathbf{a}_p^e - W_{\text{exp}} \quad (56) \end{aligned}$$

From  $\frac{\partial \Pi_R^e}{\partial \boldsymbol{\alpha}_M} = 0$ ,  $\boldsymbol{\alpha}_M$  can be solved out:

$$\boldsymbol{\alpha}_M = -\mathbf{K}_{MM}^{-1} \mathbf{K}_{Ma} \boldsymbol{a}_p^e \quad (57)$$

where

$$\begin{aligned} \mathbf{K}_{MM} &= -\iint_{A^e} (\mathbf{P}_M^T \mathbf{D}_b^{-1} \mathbf{P}_M + \mathbf{P}_T^T \mathbf{D}_s^{-1} \mathbf{P}_T) dA \\ \mathbf{K}_{Ma} &= \iint_{A^e} (\mathbf{P}_M^T \mathbf{B}_b + \mathbf{P}_T^T \mathbf{B}_s) dA \end{aligned} \quad (58)$$

Substituting Eqs. (57) into Eqs. (51) and (54),  $\mathbf{M}$  and  $\mathbf{T}$  can be obtained.

### 2.3 The new flat-shell element GMST18

Assembling Eqs. (12) and (48) according to the DOF's sequence (Eq. (1)), we obtain the flat-shell element stiffness matrix  $\mathbf{K}^e$  in the local co-ordinates. And after transforming  $\mathbf{K}^e$  to the global coordinates by standard procedure (Zienkiewicz and Taylor 2000), the element can be used to calculate shell structures.

This element is named GMST18, to remind that it is a Generalized conforming Mindlin SemiLoof Triangular finite element with 18 DOFs.

## 3. Updated Lagrangian formulae

In incremental method, all the physical components of a structure from time 0 to time  $t$  are assumed to have been obtained. What we are interested in is the increment that occurs from time  $t$  to time  $t + \Delta t$ . The reference configuration is the configuration at time  $t$ .

The principle of virtual displacement expressed by the UL method can be written as

$$\iiint_V ({}^{t+\Delta t} \boldsymbol{\sigma}_{ij}) \delta ({}^{t+\Delta t} \boldsymbol{\varepsilon}_{ij}) dV = {}^{t+\Delta t} W \quad (59)$$

where  ${}^{t+\Delta t} \boldsymbol{\sigma}_{ij}$  and  ${}^{t+\Delta t} \boldsymbol{\varepsilon}_{ij}$  are the modified Kirchhoff stress tensor and the modified Green strain tensor, respectively.  ${}^{t+\Delta t} W$  is the virtual work done by external loadings at the time  $t + \Delta t$ .

$${}^{t+\Delta t} \boldsymbol{\sigma}_{ij} = \boldsymbol{\sigma}_{ij}^E + \Delta \boldsymbol{\sigma}_{ij} \quad (60)$$

where  $\boldsymbol{\sigma}_{ij}^E$  is the Cauchy stress tensor at the time  $t$ , and  $\Delta \boldsymbol{\sigma}_{ij}$  is the Kirchhoff stress tensor increment from time  $t$  to time  $t + \Delta t$ .

$$\begin{aligned} {}^{t+\Delta t} \boldsymbol{\varepsilon}_{ij} &= \Delta \boldsymbol{\varepsilon}_{ij} = \Delta e_{ij} + \Delta \eta_{ij} \\ \Delta e_{ij} &= \frac{1}{2} (\Delta u_{i,j} + \Delta u_{j,i}), \quad \Delta \eta_{ij} = \frac{1}{2} \Delta u_{k,i} \Delta u_{k,j} \end{aligned} \quad (61)$$

where  $\Delta e_{ij}$  and  $\Delta \eta_{ij}$  are the linear and non-linear Green strain tensor increment from time  $t$  to time  $t + \Delta t$ , respectively. And  $\Delta u_i$  is the displacement increment from time  $t$  to time  $t + \Delta t$ .

If  $\Delta t$  is small enough, the following relationship can be established

$$\Delta\sigma_{ij} = D_{ijkl}\Delta\varepsilon_{ij} \quad (62)$$

where  $D_{ijkl}$  is elastic tensor.

Substitution of Eqs. (60), (61) and (62) into (59) yields (the higher-order terms have been neglected)

$$I_1 + I_2 = ({}^{t+\Delta t}W) - I_3 \quad (63)$$

with

$$I_1 = \int_V D_{ijkl}\Delta e_{kl}\delta\Delta e_{kl}dV, \quad I_2 = \int_V \sigma_{ij}^E\delta\Delta\eta_{ij}dV, \quad I_3 = \int_V \sigma_{ij}^E\delta\Delta e_{ij}dV \quad (64)$$

where  $I_1$  is the linear increment of virtual work;  $I_2$  is the incremental virtual work relevant to the initial stresses;  $I_3$  is the incremental virtual work done by the internal forces.

For the flat-shell element in the local co-ordinates,  $I_1$ ,  $I_2$  and  $I_3$  in Eq. (63) can be rewritten in the following discrete form

$$\begin{aligned} I_1 &= \iint_{A^e} (\delta\Delta\boldsymbol{\varepsilon}_m^T \mathbf{D}_m \Delta\boldsymbol{\varepsilon}_m + \delta\Delta\boldsymbol{\kappa}^T \mathbf{D}_b \Delta\boldsymbol{\kappa} + \delta\Delta\boldsymbol{\gamma}^T \mathbf{D}_s \Delta\boldsymbol{\gamma}) dA \\ I_2 &= \iint_{A^e} \delta\Delta\mathbf{w}'^T \bar{\mathbf{N}}^E \Delta\mathbf{w}' dA \\ I_3 &= \iint_{A^e} (\delta\Delta\mathbf{N}_m^E + \delta\Delta\mathbf{M}^E + \delta\Delta\mathbf{T}^E) dA \end{aligned} \quad (65)$$

where  $\Delta$  means the increment of relevant variables;  $\Delta\boldsymbol{\varepsilon}_m$  is the linear increment of the membrane strain and given by

$$\Delta\boldsymbol{\varepsilon}_m = \left[ \frac{\partial\Delta u}{\partial x} \quad \frac{\partial\Delta u}{\partial y} \quad \frac{\partial\Delta v}{\partial x} \right]^T = \mathbf{B}_m \Delta\mathbf{a}_m^e \quad (66)$$

$\Delta\boldsymbol{\kappa}$  is the linear increment of the curvature vector given in Eq. (46);  $\Delta\boldsymbol{\gamma}$  is the increment of the transverse shear strain vector given in Eq. (18);

$$\Delta\mathbf{w}' = \begin{Bmatrix} \frac{\partial\Delta w}{\partial x} \\ \frac{\partial\Delta w}{\partial y} \end{Bmatrix} = \begin{Bmatrix} F'_{\lambda,x} \\ F'_{\lambda,y} \end{Bmatrix} \mathbf{CL} \Delta\mathbf{a}_p^e = \mathbf{B}_G \Delta\mathbf{a}_p^e \quad \text{with} \quad \mathbf{B}_G = \begin{Bmatrix} F'_{\lambda,x} \\ F'_{\lambda,y} \end{Bmatrix} \mathbf{CL} \quad (67)$$

$$\bar{\mathbf{N}}^E = \begin{bmatrix} \int_{-h/2}^{h/2} \sigma_x^E dz & \int_{-h/2}^{h/2} \tau_{xy}^E dz \\ \int_{-h/2}^{h/2} \tau_{xy}^E dz & \int_{-h/2}^{h/2} \sigma_y^E dz \end{bmatrix} = \begin{bmatrix} N_x^E & N_{xy}^E \\ N_{xy}^E & N_y^E \end{bmatrix} \quad (68)$$

$\mathbf{N}_m^E$ ,  $\mathbf{M}^E$  and  $\mathbf{T}^E$  are the membrane force, bending moment and shear force vectors at the time  $t$ , respectively.

$$\mathbf{N}_m^E = [N_x^E \quad N_y^E \quad N_{xy}^E]^T, \quad \mathbf{M}^E = [M_x^E \quad M_y^E \quad M_{xy}^E]^T, \quad \mathbf{T}^E = [T_x^E \quad T_y^E]^T \quad (69)$$

Substitution of the geometric relation Eqs. (18), (46) and (66) into (65) yields

$$\begin{aligned}
I_1 &= \delta\Delta\mathbf{a}_m^e \left( \iint_{A^e} \mathbf{B}_m^T \mathbf{D}_m \mathbf{B}_m dA \right) \Delta\mathbf{a}_m^e + \delta\Delta\mathbf{a}_p^e \left( \iint_{A^e} (\mathbf{B}_b^T \mathbf{D}_b \mathbf{B}_b + \mathbf{B}_s^T \mathbf{D}_s \mathbf{B}_s) dA \right) \Delta\mathbf{a}_p^e \\
I_2 &= \delta\Delta\mathbf{a}_p^e \left( \iint_{A^e} \mathbf{B}_G^T \bar{\mathbf{N}}^E \mathbf{B}_G dA \right) \Delta\mathbf{a}_p^e \\
I_3 &= \delta\Delta\mathbf{a}_m^e \left( \iint_{A^e} \mathbf{B}_m^T \mathbf{N}_m^E dA \right) + \delta\Delta\mathbf{a}_p^e \left( \iint_{A^e} (\mathbf{B}_b^T \mathbf{M}^E + \mathbf{B}_s^T \mathbf{T}^E) dA \right)
\end{aligned} \quad (70)$$

And  ${}^{t+\Delta t}W$  can be rewritten as

$${}^{t+\Delta t}W = \delta\Delta\mathbf{a}_m^e ({}^{t+\Delta t}\mathbf{R}_m^e) + \delta\Delta\mathbf{a}_p^e ({}^{t+\Delta t}\mathbf{R}_p^e) \quad (71)$$

where  ${}^{t+\Delta t}\mathbf{R}_m^e$  and  ${}^{t+\Delta t}\mathbf{R}_p^e$  are the equivalent nodal force vectors at the time  $t + \Delta t$  of the membrane element and plate bending element, respectively.

$\delta\Delta\mathbf{a}_m^e$  and  $\delta\Delta\mathbf{a}_p^e$  are arbitrary. Thus, according to the variational principle and Eqs. (63), (70) and (71), we can obtain the element incremental equations in the local co-ordinates:

$$\begin{bmatrix} \mathbf{K}_m^e & \mathbf{0} \\ \mathbf{0} & \mathbf{K}_p^e + \mathbf{K}_\sigma^e \end{bmatrix} \begin{Bmatrix} \Delta\mathbf{a}_m^e \\ \Delta\mathbf{a}_p^e \end{Bmatrix} = \begin{Bmatrix} {}^{t+\Delta t}\mathbf{R}_m^e \\ {}^{t+\Delta t}\mathbf{R}_p^e \end{Bmatrix} - \begin{Bmatrix} \Psi_m^e \\ \Psi_p^e \end{Bmatrix} \quad (72)$$

where  $\mathbf{K}_m^e$  is the linear stiffness matrix of the membrane element and given by Eq. (8);  $\mathbf{K}_p^e$  is the linear stiffness matrix of the plate bending element and given by Eq. (48);  $\mathbf{K}_\sigma^e$  is the geometric stiffness matrix,

$$\mathbf{K}_\sigma^e = \iint_{A^e} \mathbf{B}_G^T \bar{\mathbf{N}}^E \mathbf{B}_G dA \quad (73)$$

$\Psi_m^e$  is the equivalent nodal internal force vector of the membrane element;  $\Psi_p^e$  is the equivalent nodal internal force vector of the plate bending element,

$$\Psi_m^e = \iint_{A^e} \mathbf{B}_m^T \mathbf{N}_m^E dA, \quad \Psi_p^e = \iint_{A^e} (\mathbf{B}_b^T \mathbf{M}^E + \mathbf{B}_s^T \mathbf{T}^E) dA \quad (74)$$

Rewriting (72) according to the DOF's sequence yields

$$(\mathbf{K}^e + \mathbf{K}_\sigma^e) \Delta\mathbf{a}^e = {}^{t+\Delta t}\mathbf{R}^e - \Psi^e \quad (75)$$

After transforming (75) to the global co-ordinates by standard procedure (Zienkiewicz and Taylor 2000), element GMST18 can be used to analysis the geometrically nonlinear problem of shells.

## 4. Numerical examples

The element GMST18 is introduced into the commercial finite element software ABAQUS (ABAQUS/Standard User's Manual 1998) by user element function and evaluated by three types of numerical examples: (i) plate bending; (ii) linear shell; and (iii) geometrically nonlinear shell.

### 4.1 Plate bending problems

Firstly, some standard examples are used to assess the accuracy of the new derived element TSL-T9, the plate bending component of the element GMST18. All the bending moment and shear force solutions are calculated by both the constitutive relations (50) and the hybrid enhanced procedure proposed in section 2.2.8.

4.1.1 Eigenvalues and rank

Only three eigenvalues are always zero (corresponding to the rigid body modes of the element) for various element shapes of very thin and very thick plates. The element TSL-T9 always has a proper rank. This is to say the element has no spurious zero-energy modes. We can claim that in real applications the triangular element is stable provided sufficient boundary conditions are imposed to prevent rigid body motion.

4.1.2 Patch test presented in Fig. 7

(a) Bending moment  $M_n = 1$

For the bending moments  $M_n = 1$  along the four sides, the equivalent nodal forces are directly obtained since  $\beta_n$  is linear along the sides (refer to Eq. (28b)). The computed values of  $M_x, M_y, M_{xy}, T_x$  and  $T_y$  at any point in the four elements are exact (error = 0.00%) for thick ( $h/2a = 0.1$ ) and thin ( $h/2a = 0.001$ ) plates.

(b) Twist moment  $M_{ns} = 1$

The consistent definition of  $\beta_s$  has been given in Eq. (15b). The consistent nodal forces for  $M_{ns} = 1$  are given in Fig. 7 for the arbitrary thickness-span ratio. The results obtained using the element TSL-T9 are exactly the same as those of the exact solution (error = 0.00%), except the  $M_x (= 0)$  and  $M_y (= 0)$  of thick plate ( $h/2a = 0.1$ ) in which the max discrepancy between the two solutions is less than 0.6%.

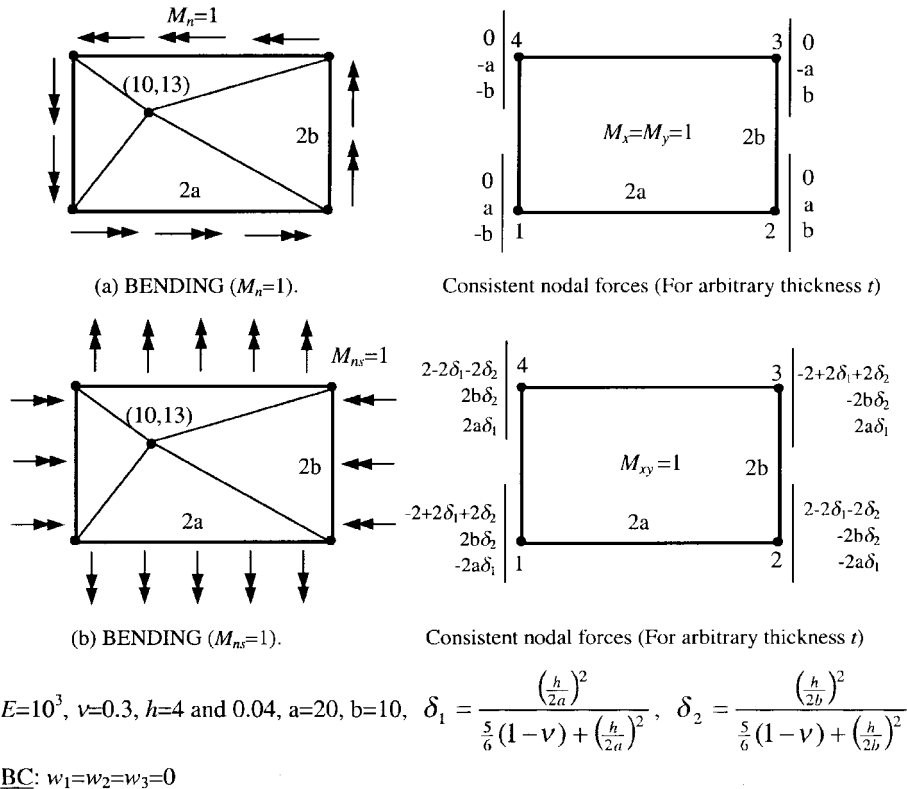


Fig. 7 Patch test: Contant bending moments

Thus, TSL-T9 passes the patch-test.

#### 4.1.3 Simply-supported and clamped square plate

Fig. 8 shows the typical meshes employed for the study of a square plate. Two simply supported cases were considered. One was soft (SS1,  $w = 0$ ) and the other was hard (SS2,  $w = \theta_n = \beta_s = 0$ ). Moreover, a clamped square plate was also considered. The thickness and side length of the plate are denoted by  $h$  and  $l$ , respectively; and the Poisson's ratio  $\nu$  of the material was assumed to be 0.3. Tables 1 to 3 present the results of the central displacements and moments subjected to a uniformly distributed load  $q = 1$  from very thin plate ( $h/l = 10^{-30}$ ) to thick plate ( $h/l = 0.1$ ). It is

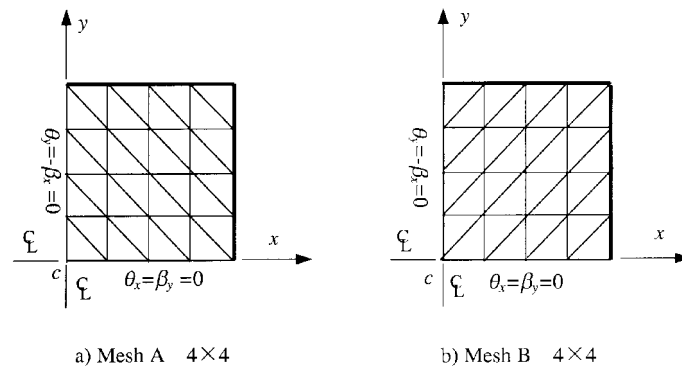


Fig. 8 Typical mesh ( $4 \times 4$ ) for  $1/4$  square plate (point  $c$  is the center of plate)

Table 1 Central displacements  $w_c/(ql^4/100D)$  and moments  $M_c/(ql^2/10)$  for the hard simply supported (SS2) square plate subjected to uniform load  $q$

$h/l$	Number Mesh type	$2 \times 2$	$4 \times 4$	$8 \times 8$	$16 \times 16$	Analytical solutions
		$w_c/(ql^4/100D)$				
$10^{-30} \sim 0.001$	Mesh A	0.4024	0.4058	0.4062	0.4062	0.4062
	Mesh B	0.4014	0.4051	0.4060	0.4062	
0.01	Mesh A	0.4026	0.4059	0.4063	0.4063	0.4064
	Mesh B	0.4016	0.4052	0.4061	0.4063	
0.1	Mesh A	0.4146	0.4214	0.4249	0.4266	0.4273
	Mesh B	0.4189	0.4233	0.4258	0.4269	
$M_c/(ql^2/10)$						
$10^{-30} \sim 0.001$	Mesh A	0.5161 <sup>c,h</sup>	0.4917 <sup>c,h</sup>	0.4830 <sup>c,h</sup>	0.4801 <sup>c,h</sup>	0.4789
	Mesh B	0.5022 <sup>c,h</sup>	0.4798 <sup>c,h</sup>	0.4781 <sup>c,h</sup>	0.4784 <sup>c,h</sup>	
0.01	Mesh A	0.5163 <sup>c</sup> /0.5161 <sup>h</sup>	0.4919 <sup>c</sup> /0.4914 <sup>h</sup>	0.4832 <sup>c</sup> /0.4827 <sup>h</sup>	0.4802 <sup>c</sup> /0.4800 <sup>h</sup>	0.4789
	Mesh B	0.5026 <sup>c</sup> /0.5022 <sup>h</sup>	0.4803 <sup>c</sup> /0.4799 <sup>h</sup>	0.4786 <sup>c</sup> /0.4782 <sup>h</sup>	0.4789 <sup>c</sup> /0.4786 <sup>h</sup>	
0.1	Mesh A	0.5301 <sup>c</sup> /0.5058 <sup>h</sup>	0.5017 <sup>c</sup> /0.4904 <sup>h</sup>	0.4872 <sup>c</sup> /0.4831 <sup>h</sup>	0.4814 <sup>c</sup> /0.4802 <sup>h</sup>	0.4789
	Mesh B	0.5276 <sup>c</sup> /0.5078 <sup>h</sup>	0.4965 <sup>c</sup> /0.4882 <sup>h</sup>	0.4845 <sup>c</sup> /0.4819 <sup>h</sup>	0.4804 <sup>c</sup> /0.4797 <sup>h</sup>	

c. Results by the Constitutive Eq. (50);

h. Results by the Hybrid-enhanced procedure proposed in section 2.2.8

Table 2 Central displacements  $w_c/(ql^4/100D)$  and moments  $M_c/(ql^2/10)$  for the soft simply supported (SS1) square plate subjected to uniform load  $q$ 

$h/l$	Number Mesh type	2 × 2	4 × 4	8 × 8	16 × 16	Analytical solutions
		$w_c/(ql^4/100D)$				
$10^{-30} \sim 0.001$	Mesh A	0.4030	0.4059	0.4062	0.4062	0.4062 (Taylor <i>et al.</i> 1993)
	Mesh B	0.4034	0.4052	0.4060	0.4062	
0.1	Mesh A	0.4154	0.4293	0.4465	0.4568	0.4617
	Mesh B	0.4239	0.4322	0.4472	0.4570	
$M_c/(ql^2/10)$						
$10^{-30} \sim 0.001$	Mesh A	0.5133 <sup>c,h</sup>	0.4909 <sup>c,h</sup>	0.4828 <sup>c,h</sup>	0.4801 <sup>c,h</sup>	0.4789
	Mesh B	0.5074 <sup>c,h</sup>	0.4809 <sup>c,h</sup>	0.4783 <sup>c,h</sup>	0.4785 <sup>c,h</sup>	
0.1	Mesh A	0.5279 <sup>c</sup> /0.5050 <sup>h</sup>	0.5085 <sup>c</sup> /0.4976 <sup>h</sup>	0.5066 <sup>c</sup> /0.5026 <sup>h</sup>	0.5085 <sup>c</sup> /0.5073 <sup>h</sup>	0.5096
	Mesh B	0.5387 <sup>c</sup> /0.5183 <sup>h</sup>	0.5055 <sup>c</sup> /0.4971 <sup>h</sup>	0.5040 <sup>c</sup> /0.5013 <sup>h</sup>	0.5074 <sup>c</sup> /0.5067 <sup>h</sup>	

c. Results by the Constitutive Eq. (50);

h. Results by the Hybrid-enhanced procedure proposed in section 2.2.8

Table 3 Central displacements  $w_c/(ql^4/100D)$  and moments  $M_c/(ql^2/10)$  for the clamped square plate subjected to uniform load  $q$ 

$h/l$	Number Mesh type	2 × 2	4 × 4	8 × 8	16 × 16	Analytical solutions
		$w_c/(ql^4/100D)$				
$10^{-30} \sim 0.001$	Mesh A	0.1077	0.1220	0.1254	0.1263	0.1265
	Mesh B	0.1229	0.1254	0.1263	0.1265	
0.01	Mesh A	0.1078	0.1222	0.1256	0.1264	0.1267
	Mesh B	0.1230	0.1256	0.1263	0.1267	
0.1	Mesh A	0.1199	0.1402	0.1471	0.1495	0.1499
	Mesh B	0.1426	0.1464	0.1487	0.1499	
$M_c/(ql^2/10)$						
0.001	Mesh A	0.2380 <sup>c,h</sup>	0.2343 <sup>c,h</sup>	0.2306 <sup>c,h</sup>	0.2295 <sup>c,h</sup>	0.2291 (Taylor <i>et al.</i> 1993)
	Mesh B	0.2909 <sup>c,h</sup>	0.2386 <sup>c,h</sup>	0.2309 <sup>c,h</sup>	0.2294 <sup>c,h</sup>	
0.1	Mesh A	0.2473 <sup>c</sup> /0.2230 <sup>h</sup>	0.2448 <sup>c</sup> /0.2335 <sup>h</sup>	0.2374 <sup>c</sup> /0.2333 <sup>h</sup>	0.2337 <sup>c</sup> /0.2325 <sup>h</sup>	0.231 (Taylor <i>et al.</i> 1993)
	Mesh B	0.3015 <sup>c</sup> /0.2839 <sup>h</sup>	0.2545 <sup>c</sup> /0.2468 <sup>h</sup>	0.2390 <sup>c</sup> /0.2365 <sup>h</sup>	0.2339 <sup>c</sup> /0.2332 <sup>h</sup>	

c. Results by the Constitutive Eq. (50);

h. Results by the Hybrid-enhanced procedure proposed in section 2.2.8

obvious that the proposed element, TSL-T9, is a high precision and fast convergence element whether it is used for thin or thick plate analysis. No shear locking happens in thin plate limit. The comparisons of the present results with those obtained by other element models, DKT (Batoz, Bathe

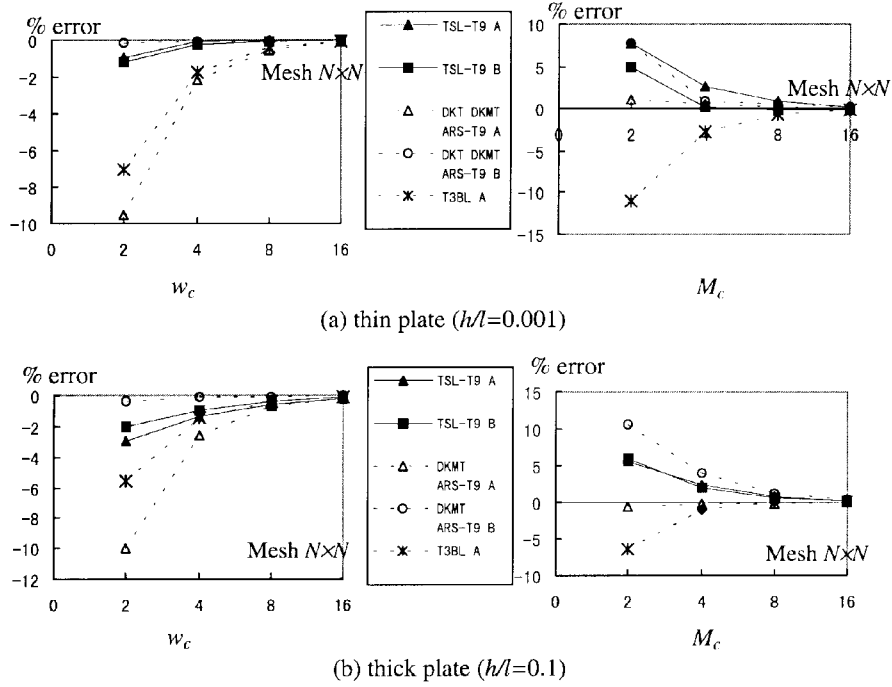


Fig. 9 The percentage error of central deflection  $w_c$  and moment  $M_c$  for hard simply supported (SS2) square plates

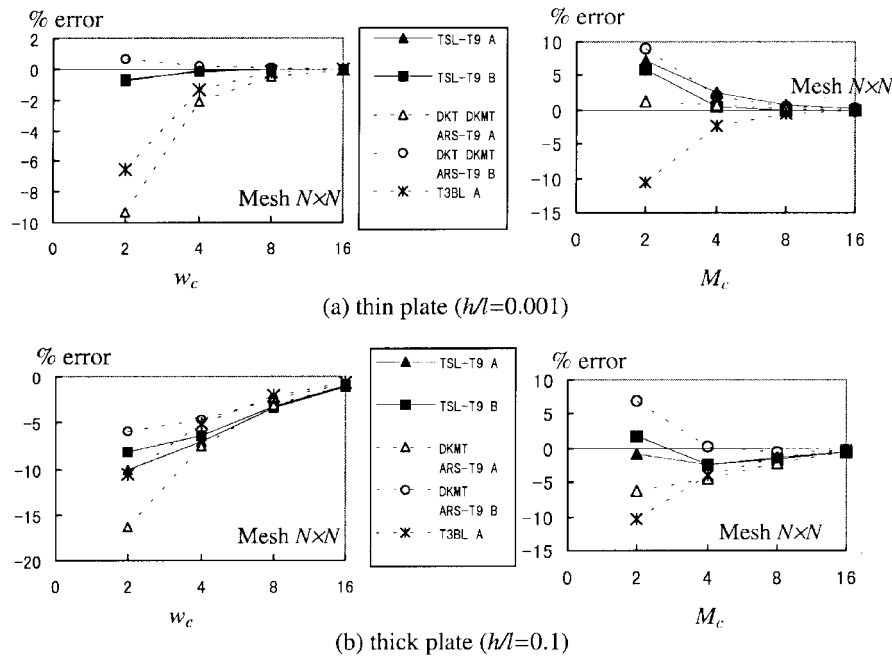


Fig. 10 The percentage error of central deflection  $w_c$  and moment  $M_c$  for soft simply supported (SS1) square plates

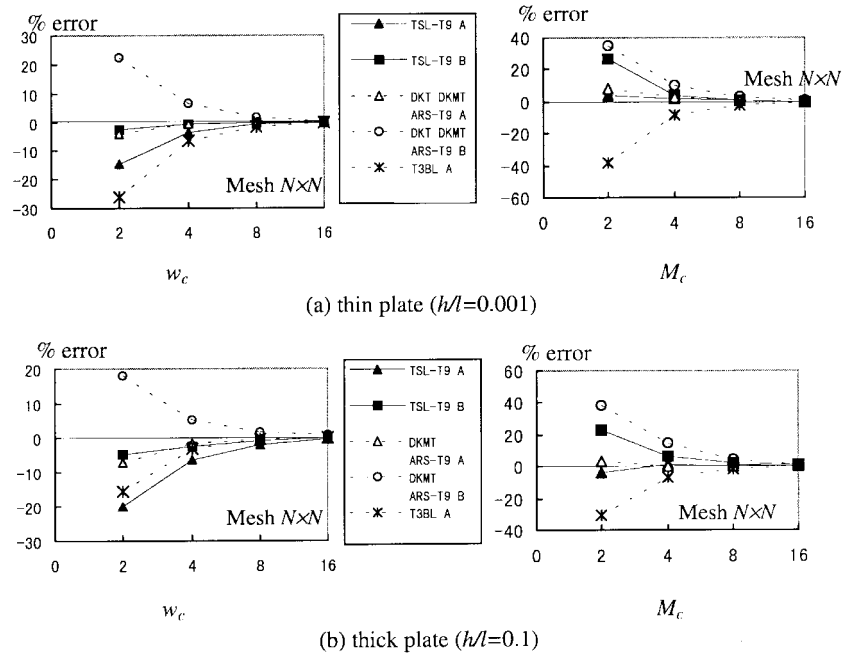


Fig. 11 The percentage error of central deflection  $w_c$  and moment  $M_c$  for clamped square plates

and Ho 1980), DKMT (Katili 1993), ARS-T9 (Soh, Long and Cen 1999), T3BL (Taylor and Auricchio 1993), are also plotted in Fig. 9 to 11. (Note: for present element TSL-T9, only hybrid-enhanced moment solutions are plotted). It also shows that present element can provide similar solutions under different mesh type A and B for most cases, while significantly differences exist in other elements.

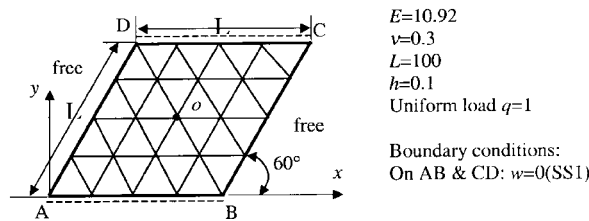


Fig. 12 Razzaque's skew plate  $4 \times 4$  mesh

#### 4.1.4 Skew plates

(a) Fig. 12 shows a  $60^\circ$  skew plate which was originally studied by Razzaque (1973). This plate was simply supported (SS1) on two opposite edges and free on the other two edges. The results obtained using the present element TSL-T9 and other triangular or quadrilateral elements are shown in Table 4 and Fig. 13. It shows that TSL-T9 exhibits excellent performance in both displacement and moment solutions.

(b) The simply supported (SS1) skew plate illustrated in Fig. 14 has been solved by (Morley 1963) for the limiting Kirchhoff-Germain assumptions. Babuška and Scapolla (1989) also solved

Table 4 Results for the Razzaque’s skew plate

Mesh $N \times N$	TSL-T9	MiSP3+ (Ayad <i>et al.</i> 2001)	MiSP3 (Ayad <i>et al.</i> 1998)	DKT DKMT ARS-T9	MITC4 (Bathe <i>et al.</i> 1985)	MiSP4 (Ayad <i>et al.</i> 1998)	MMiSP4 (Ayad <i>et al.</i> 1998)	ARS-Q12 (Soh <i>et al.</i> 2001)
(a) Central deflection $w_o \times 10^{-9}$								
$2 \times 2$	0.7191	0.6215	0.5663	0.6327	0.3856	0.5120	0.2979	0.6666
$4 \times 4$	0.7735	0.7610	0.7400	0.7539	0.6689	0.7259	0.6668	0.7691
$8 \times 8$	0.7865	0.7860	0.7805	0.7816	0.7560	0.7781	0.7604	0.7876
$16 \times 16$	0.7898	0.7899	0.7894	0.7886	0.7797	0.7894	0.7832	0.7920
Exact (Razzaque 1973)				0.7945				
(b) Central moment $M_y \times 10^{-3}$								
$2 \times 2$	0.9937 <sup>c,h</sup>	0.6767	0.6668	0.9145	0.3778	0.6066	0.4687	0.9246
$4 \times 4$	0.9760 <sup>c,h</sup>	0.9100	0.8930	0.9559	0.7706	0.8774	0.7704	0.9595
$8 \times 8$	0.9651 <sup>c,h</sup>	0.9501	0.9454	0.9601	0.9070	0.9423	0.9052	0.9605
$16 \times 16$	0.9613 <sup>c,h</sup>	0.9581	0.9571	0.9600	0.9472	0.9567	0.9466	0.9601
Exact (Razzaque 1973)				0.9589				

c. Results by the Constitutive Eq. (50);

h. Results by the Hybrid-enhanced procedure proposed in section 2.2.8

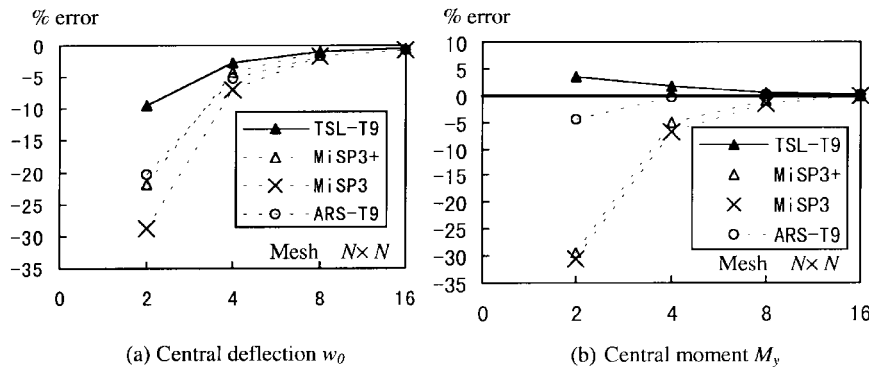


Fig. 13 The percentage error of central deflection  $w_o$  and moment  $M_y$  for a Razzaque’s skew plate (Triangular elements)

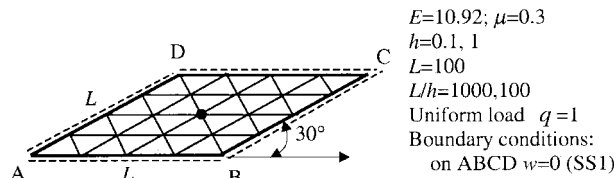


Fig. 14 Morley’s skew plate  $4 \times 4$  mesh

this problem as a 3-D elastic case. The results obtained using TSL-T9 and some other elements are presented in Tables 5 through 6. The accuracy and reliability of the proposed element is again clearly illustrated.

Table 5 Displacement and principal moments at the center of Morley's acute skew plate ( $L/h = 1000$ )

Mesh $N \times N$	TSL-T9	ARS-T9 (Soh <i>et al.</i> 1999)	T3BL (Taylor <i>et al.</i> 1993)	T3BL(R) (Taylor <i>et al.</i> 1993)	MITC4 (Bathe <i>et al.</i> 1985)	Q4BL (Zienkiewicz <i>et al.</i> 1993)	DKMQ (Katili 1993)	ARS-Q12 (Soh <i>et al.</i> 2001)
(a) Central deflection $w_o/(qL^4/1000D)$								
$4 \times 4$	0.453	0.453	0.421	0.489	0.358	0.512	0.760	0.756
$8 \times 8$	0.422	0.424	0.415	0.439	0.343	0.439	0.507	0.506
$16 \times 16$	0.417	0.419	0.414	0.426	0.343	0.429	0.443	0.442
$32 \times 32$	0.415	0.417	0.413	0.421	0.362	0.424	0.425	0.424
Morley (Morley 1963)	0.408							
(b) Central max principal moment $M_{\max}/(qL^2/100)$								
$4 \times 4$	2.189 <sup>c,h</sup>	2.217	1.722	1.820	1.669	2.012	2.339	2.314
$8 \times 8$	1.940 <sup>c,h</sup>	1.983	1.893	1.912	1.733	1.990	2.074	2.069
$16 \times 16$	1.940 <sup>c,h</sup>	1.951	1.912	1.942	1.717	1.967	1.984	1.985
$32 \times 32$	1.928 <sup>c,h</sup>	1.934	1.918	1.940	1.777	1.953	1.950	1.950
Morley (Morley 1963)	1.910							
(b) Central min principal moment $M_{\min}/(qL^2/100)$								
$4 \times 4$	1.425 <sup>c,h</sup>	1.429	0.955	0.964	0.921	1.133	1.751	1.730
$8 \times 8$	1.068 <sup>c,h</sup>	1.116	1.090	1.099	0.957	1.164	1.276	1.271
$16 \times 16$	1.118 <sup>c,h</sup>	1.124	1.100	1.125	0.874	1.152	1.166	1.168
$32 \times 32$	1.110 <sup>c,h</sup>	1.106	1.100	1.125	0.923	1.140	1.137	1.136
Morley (Morley 1963)	1.080							

c. Results by the Constitutive Eq. (50);

h. Results by the Hybrid-enhanced procedure proposed in section 2.2.8

Table 6 Displacement and principal moments at the center of Morley's acute skew plate ( $L/h = 100$ )

Mesh $N \times N$	TSL-T9	ARS-T9 (Soh <i>et al.</i> 1999)	T3BL (Taylor <i>et al.</i> 1993)	T3BL(R) (Taylor <i>et al.</i> 1993)	MITC4 (Bathe <i>et al.</i> 1985)	Q4BL (Zienkiewicz <i>et al.</i> 1993)	DKMQ (Katili 1993)	ARS-Q12 (Soh <i>et al.</i> 2001)
(a) Central deflection $w_o/(qL^4/1000D)$								
$4 \times 4$	0.453	0.454	0.422	0.490	0.359	0.513	0.757	0.754
$8 \times 8$	0.423	0.425	0.417	0.440	0.357	0.440	0.504	0.503
$16 \times 16$	0.418	0.421	0.418	0.428	0.383	0.431	0.441	0.440
$32 \times 32$	0.417	0.419	0.420	0.424	0.404	0.427	0.423	0.423
Morley (Morley 1963)	0.408							
3-D (Babuška and Scapolla 1989)	0.423							
(b) Central max principal moment $M_{\max}/(qL^2/100)$								
$4 \times 4$	2.190 <sup>c</sup> /2.188 <sup>h</sup>	2.217	1.724	1.820	1.670	2.014	2.330	2.310
$8 \times 8$	1.942 <sup>c</sup> /1.939 <sup>h</sup>	1.983	1.893	1.913	1.782	1.992	2.073	2.067
$16 \times 16$	1.943 <sup>c</sup> /1.940 <sup>h</sup>	1.952	1.922	1.946	1.844	1.973	1.984	1.983
$32 \times 32$	1.934 <sup>c</sup> /1.932 <sup>h</sup>	1.940	1.937	1.947	1.894	1.962	1.945	1.947
Morley (Morley 1963)	1.910							
(b) Central min principal moment $M_{\min}/(qL^2/100)$								
$4 \times 4$	1.427 <sup>c</sup> /1.425 <sup>h</sup>	1.430	0.956	0.965	0.921	1.132	1.740	1.723
$8 \times 8$	1.074 <sup>c</sup> /1.073 <sup>h</sup>	1.118	1.089	1.100	0.999	1.164	1.267	1.267
$16 \times 16$	1.121 <sup>c</sup> /1.120 <sup>h</sup>	1.127	1.107	1.127	1.046	1.155	1.166	1.169
$32 \times 32$	1.118 <sup>c</sup> /1.117 <sup>h</sup>	1.124	1.121	1.132	1.076	1.149	1.135	1.137
Morley (Morley 1963)	1.910							

c. Results by the Constitutive Eq. (50);

h. Results by the Hybrid-enhanced procedure proposed in section 2.2.8

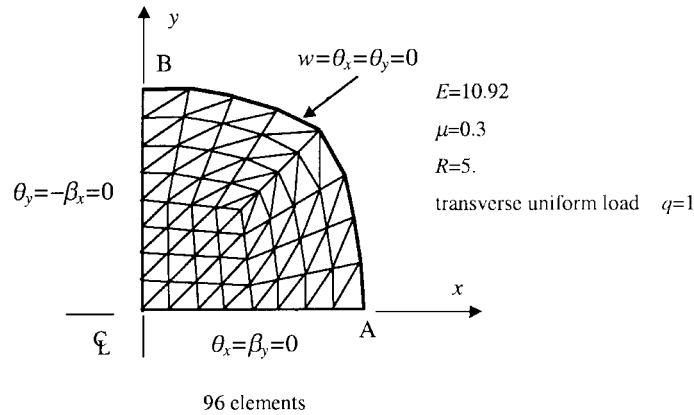


Fig. 15 The typical mesh for 1/4 circular plate

#### 4.1.5 Circular plate

A clamped circular plate subjected to a uniformly distributed load  $q = 1$  is showed in Fig. 15. The radius, Young's modulus and Poisson's ratio of the plate were assumed to be 5, 10.92 and 0.3, respectively. In Figs. 16 through 19 show the results of bending moments  $M_r$  and  $M_\theta$ , shear force  $T_r$  and displacement  $w_r$ , respectively, on a radius for the thin and thick plates. All results were obtained using a mesh with 96 elements. It is obvious that the results obtained using the proposed element are in excellent agreement with those of the exact solutions, except the shear forces obtained by the constitutive Eq. (50) in thin-plate analysis. It also demonstrates that better stress solutions can be obtained by the proposed hybrid-enhanced procedure.

### 4.2 Linear shell problems

#### 4.2.1 Scordelis-Lo roof

The cylindrical shell in Fig. 20 is supported by a rigid diaphragm at two ends and loaded vertically by its uniform dead weight. Because the shell is symmetric, only a quarter is taken for calculation. The results of GMST18, the following ABAQUS (ABAQUS/Standard User's Manual 1998) elements:

- (i) STRI3: 3-node, 18-DOF, triangular, flat-shell element for thin shells;
- (ii) S3R: 3-node, 18-DOF, triangular, three-dimension degenerate element with reduced integration for general shells and some other models are given in Table 7. It can be seen that better accuracy can be obtained by proposed element GMST18.

#### 4.2.2 Twisted cantilever beam

A twisted cantilever beam is shown in Fig. 21. The free end is twisted  $90^\circ$  from the clamped end. Two types of load are applied to the free end of the beam:  $P = 1.0, Q = 0.0$  and  $P = 0.0, Q = 1.0$ . The displacements in the direction of the load are reported in Table 8. Excellent results can be again obtained by GMST18.

#### 4.2.3 Hemispherical shell

As shown in Fig. 22, a hemispherical shell with hole at the top is under two opposite radial concentrated loads at point A and B. The results of the radial deflection at load point are given in Table 9.

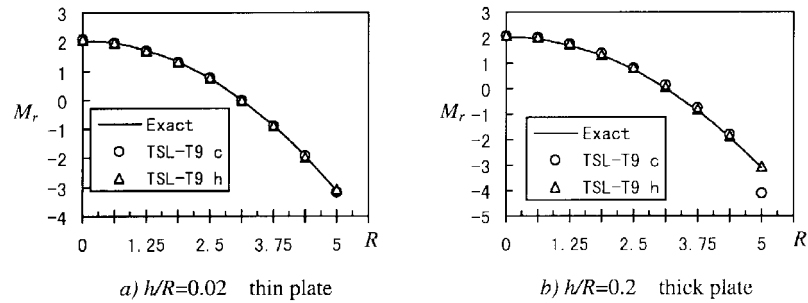


Fig. 16 Bending moment  $M_r$  along the radius of a clamped circular plate subjected to uniform loading

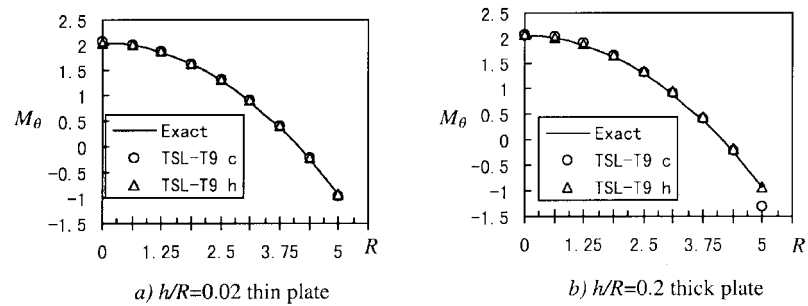


Fig. 17 Bending moment  $M_\theta$  along the radius of a clamped circular plate subjected to uniform loading.

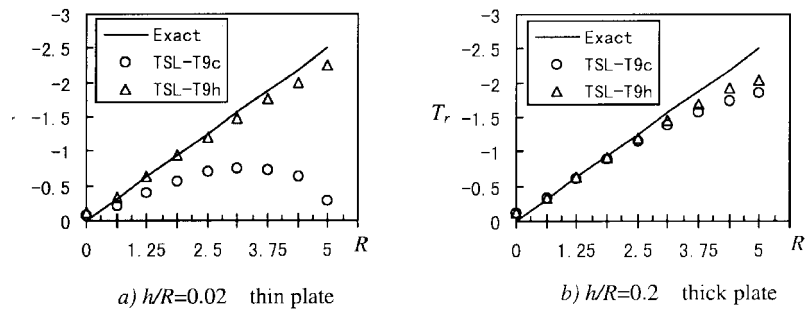


Fig. 18 Shear force  $T_r$  along the radius of a clamped circular plate subjected to uniform loading

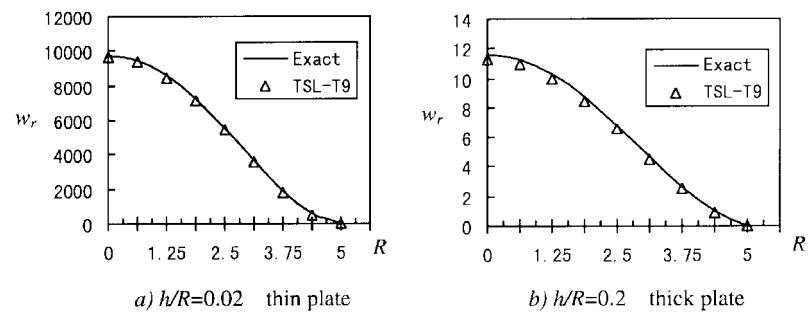


Fig. 19 Deflection  $w_r$  along the radius of a clamped circular plate subjected to uniform loading

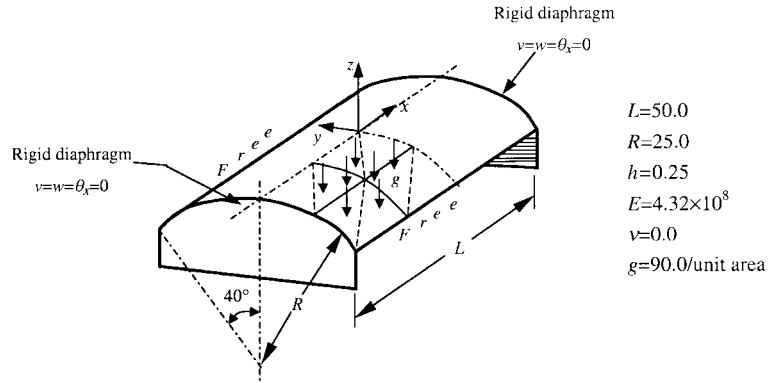


Fig. 20 Scordelis-Lo roof

Table 7 Vertical displacement at the midpoint of free edge for Scordelis-Lo roof

Mesh	Guan and Tang 1992	DKT-CST-15RB (Carpenter, Stolarski and Belytschko 1986)	Olson and Bearden 1979	STR13	S3R	GMST18
2 × 2	0.3078	0.2976	0.3809	0.3310	0.2390	0.3349
4 × 4	0.3033	0.2144	0.2942	0.2221	0.2150	0.2943
6 × 6	–	0.2428	–	0.2464	0.2438	0.2946
8 × 8	–	0.2622	–	0.2642	0.2627	0.2965
10 × 10	–	0.2737	0.2970	0.2751	0.2742	0.2978
Deep shell solution (Parisch 1979)				0.3008		

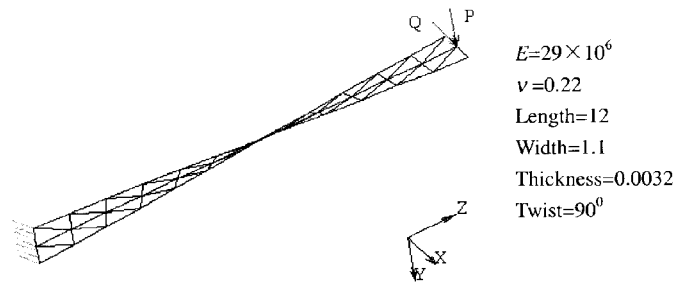


Fig. 21 Twisted beam divided into 2 × 12 mesh

### 4.3 Geometrically nonlinear shell problems

All nonlinear examples in this section are solved by Newton-Raphson method used in ABAQUS.

#### 4.3.1 Post-buckling analysis of a square plate

As shown in Fig. 23, a square plate is controlled by four clamps along each edge. Thus, the displacements in the control directions are uniform. Only a quarter of the plate using 4 × 4 mesh

Table 8 Deflection at the free edge of a cantilever twist beam

Mesh	STRI3	S3R	RTS18 (Wanji, Cheung 1999)	GMST18
Load case 1: P = 1, Q = 0				
2 × 4	59.08	663.7	851.0	875.3
2 × 8	455.6	1190	1238	1282
2 × 12	917.7	1255	1280	1293
2 × 16	1145	1275	1290	1295
Exact (Wanji and Cheung 1999)		1294		
Load case 2: P = 0, Q = 1				
2 × 4	185.6	2479	3727	3618
2 × 8	1742	4891	5117	5226
2 × 12	3678	5093	5238	5269
2 × 16	4642	5153	5268	5276
Exact (Wanji and Cheung 1999)		5256		

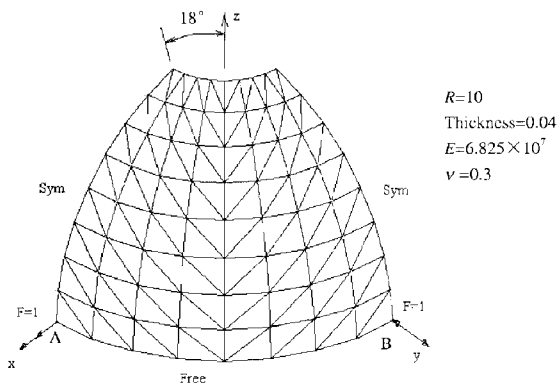


Fig. 22 Hemispherical shell with hole at the top, mesh 8 × 8

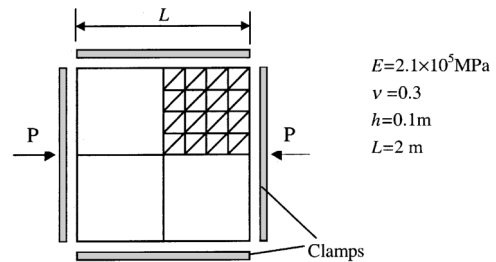


Fig. 23 Post-buckling problem for a square plate

Table 9 Radial deflection at point A of the spherical under concentrated loads at A and B

Mesh	STRI3	S3R	RTS18 (Wanji, Cheung 1999)	Providas and Kattis 2000	GMST18
4 × 4	0.094	0.055	0.091	0.095	0.082
8 × 8	0.094	0.084	0.096	0.093	0.092
16 × 16	0.093	0.092	0.094 (14 × 14)	—	0.093
64 × 64	0.093	0.093	—	—	0.094
Exact (Wanji and Cheung 1999)			0.094		

division is analyzed because of symmetry. According to the series method presented by (Budiansky 1974), the critical load and post-buckling path are given by

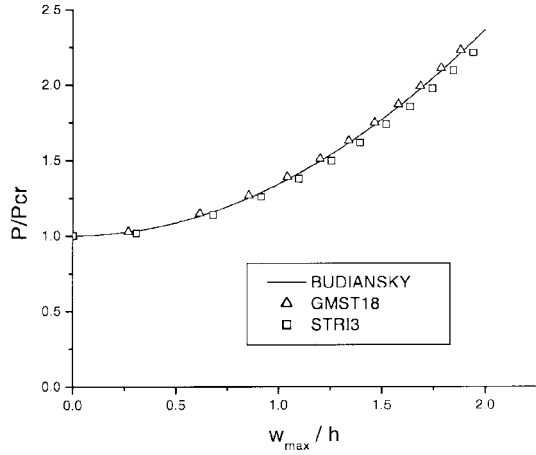


Fig. 24 Post-buckling path for a square plate, mesh  $4 \times 4$

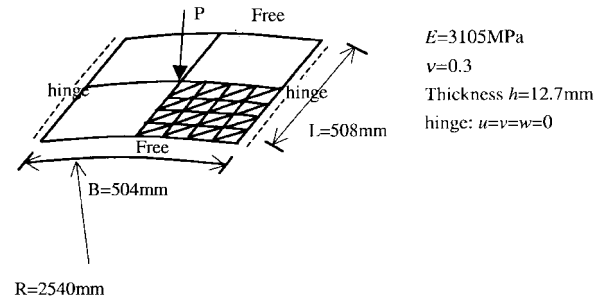


Fig. 25 A hinged cylindrical shell, mesh  $4 \times 4$

$$P_{cr} = \frac{4\pi^2 D}{L} \quad \text{and} \quad \frac{P}{P_{cr}} = 1 + \frac{3}{8}(1 - \nu^2) \left( \frac{w_{\max}}{h} \right)^2$$

where  $w_{\max}$  is the central deflection of square plate. The post-buckling paths obtained by elements GMST18 and STRI3 are plotted in Fig. 24. It can be seen that the results of GMST18 are more consistent with Budiansky's solutions than those of STRI3.

#### 4.3.2 Post-buckling analysis of a cylindrical shell subjected to a concentrated load

Fig. 25 shows a cylindrical shell subjected to a central vertical concentrated load  $P$ . The displacement loading is adopted in this example. Total number of incremental steps is 200. And the displacement step length is fixed in each step. The post-buckling path obtained by two elements GMST18 and STRI3 (under  $4 \times 4$  and  $8 \times 8$  mesh divisions) are plotted together in Fig. 26. It can be seen that all curves are in agreement with each other.

The critical load obtained by both elements under different mesh divisions is also given in Fig. 27 and Table 10. It shows that the proposed element GMST18 possesses better convergence. Furthermore, less time is needed when using element GMST18 under the same hardware and software conditions (Table 11).

## 5. Conclusions

A new 18-DOF triangular flat-shell element GMST18 has been formulated by using a new derived thin-thick plate element, TSL-T9, based on semiLoof constrains (Long 1993) and rational shear interpolation approach (Soh, Long and Cen 1999). The membrane part is modeled by the generalized conforming membrane element, GT9 (Long and Xu 1994), with rigid rotational freedoms. Furthermore, a simple hybrid procedure is suggested to improve the stress solutions, and the Updated Lagrangian formulae are also established for the geometrically nonlinear problems. The potential accuracy and versatility of the said elements have been illustrated using various numerical examples, which show that

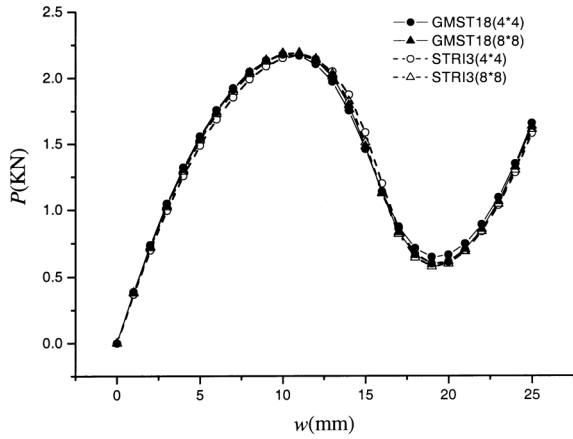


Fig. 26 Load-central deflection curve for a hinged cylindrical shell subjected to a central vertical concentrated load

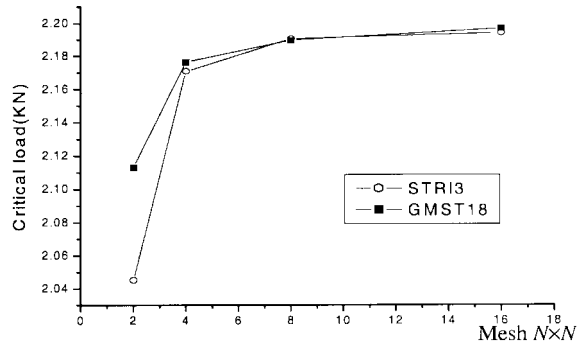


Fig. 27 Critical load for different mesh divisions for a hinged cylindrical shell

Table 10 Critical load (KN) under different mesh divisions for a simply-supported cylindrical shell

Mesh $N \times N$	STRI3	GMST18
$2 \times 2$	2.0452	2.1132
$4 \times 4$	2.1708	2.1764
$8 \times 8$	2.1904	2.1896
$16 \times 16$	2.1940	2.1968
Saleeb, Chang, Graf and Yingyeunyong 1990		2.20
Hughes and Liu 1981		2.20
Bathe and Bolourchi 1980		2.24
To and Liu 1995		2.30

Table 11 The CPU time used for post-buckling problem of a cylindrical shell (Mesh  $16 \times 16$ )

Element	No. of incremental steps	Time (s)
GMST18	200	298
STRI3	200	425

1. Element GMST18 possesses excellent performance in the analysis of very thin to thick plate and shell problems;
2. No shear locking takes place when the thickness of the shells approaches zero. And no membrane locking and hourglass happen after adopting usual numerical techniques.
3. The hybrid-enhanced procedure can improve stress solutions obviously.

4. Element GMST18 exhibits better efficiency and accuracy than the same type model used in ABAQUS.

Element GMST18 also possesses excellent performance in the analysis of laminated composite shells and smart structures. This will be introduced in another paper.

## Acknowledgements

This study was supported by the Natural Science Foundation of China (Project no. 10272063), Basic Science Research Foundation (JC2002003) of Tsinghua University, China Postdoctoral Science Foundation and the Special Foundation for the Author of the Nationwide (China) Excellent Doctoral Dissertation.

## References

- ABAQUS/Standard User's Manual, Version 5.8* (1998), Hibbitt, Karlsson & Sorensen, Inc.: Rawtucket, Rhode Island.
- Allman, D.J. (1984), "A compatible triangular element including vertex rotations for plane elasticity analysis", *Comput. Struct.*, **19**(1-2), 1-8.
- Allman, D.J. (1988), "Evaluation of the constant triangle with drilling rotations", *Int. J. Numer. Meth. Eng.*, **50**, 25-69.
- Ayad, R., Dhatt, G. and Batoz, J.L. (1998), "A new hybrid-mixed variational approach for Reissner-Mindlin plates: The MiSP model", *Int. J. Numer. Meth. Eng.*, **42**, 1149-1179.
- Ayad, R., Rigolot, A. and Talbi, N. (2001), "An improved three-node hybrid-mixed element for Mindlin/Reissner plates", *Int. J. Numer. Meth. Eng.*, **51**, 919-942.
- Babuška, I. and Scapolla, T. (1989), "Benchmark computation and performance evaluation for a rhombic plate bending problem", *Int. J. Numer. Meth. Eng.*, **28**, 155-179.
- Badiansky, B. (1974), "Theory of buckling and post-buckling behavior of elastic structure", In: *Advances in Applied Mechanics*, New York: Academic Press.
- Bathe, K.J. and Bolourchi, S. (1980), "A geometric and material nonlinear plate and shell element", *Comput. Struct.*, **21**, 367-383.
- Bathe, K.J. and Dvorkin, E. (1985), "Short communication - a four node plate bending element based on Mindlin/Reissner plate theory and mixed interpolation", *Int. J. Numer. Meth. Eng.*, **21**, 367-383.
- Batoz, J.L., Bathe, K.J. and Ho, W.J. (1980), "A Study of three-node triangular plate bending elements", *Int. J. Numer. Meth. Eng.*, **15**, 1771-1812.
- Batoz, J.L. and Lardeur, P. (1989), "A discrete shear triangular nine d.o.f. element for the analysis of thick to very thin plates", *Int. J. Numer. Meth. Eng.*, **29**, 533-560.
- Batoz, J.L. and Katili, I. (1992), "On a simple triangular Reissner/Mindlin plate element based on incompatible modes and discrete constrains", *Int. J. Numer. Meth. Eng.*, **35**, 1603-1632.
- Bazeley, G.P., Cheung, Y.K., Irons, B.M. and Zienkiewicz, O.C. (1965), "Triangular elements in bending conforming and non-conforming solutions", *Proc. Conf. Matrix Methods in Struct. Mech.*, Air Force Institute of Technology, Wright-Patterson A.F. Base, OH, 547-576.
- Carpenter, N., Stolarski, H. and Belytschko, T. (1986), "Improvements in 3-node triangular shell elements", *Int. J. Numer. Meth. Eng.*, **23**, 1643-1667.
- Cheung, Y.K. and Wanji, C. (1995), "Refined nine-parameter triangular thin plate bending element by using refined direct stiffness method", *Int. J. Numer. Meth. Eng.*, **38**, 283-298.
- Darendeliler, H., Oral, S. and Turgut, A. (1999), "A pseudo-layered, elastic-plastic, flat-shell finite element",

- Comput. Meth. Appl. Mech. Eng.*, **174**, 211-218.
- Felippa, C.A. and Alexander, S. (1992), "Membrane triangles with corner drilling freedom - III Implementation and performance evolution", *Finite Elements in Analysis and Design*, **12**, 203-239.
- Fish, J. and Belytshko, T. (1992), "Stabilized rapidly convergent 18-degree-of-freedom flat shell triangular element", *Int. J. Numer. Meth. Eng.*, **33**, 149-162.
- Guan, Y. and Tang, L. (1992), "A quasi-conforming nine-node degenerated shell finite element", *Finite Elements in Analysis and Design*, **11**, 165-176.
- Hughes, T.J.R. and Liu, W.K. (1981), "Nonlinear finite element analysis of shells, Part I: Three dimensional shells", *Comput. Method Appl. Mech. Eng.*, **26**, 331-362.
- Katili, I. (1993), "A new discrete Kirchhoff-Mindlin element based on Mindlin-Reissner plate theory and assumed shear strain fields - Part I: An extended DKT element for thick-plate bending analysis", *Int. J. Numer. Meth. Eng.*, **36**, 1859-1883.
- Katili, I. (1993), "A new discrete Kirchhoff-Mindlin element based on Mindlin-Reissner plate theory and assumed shear strain fields Part II: An extended DKQ element for thick-plate bending analysis", *Int. J. Numer. Meth. Eng.*, **36**, 1885-1908.
- Long, Y.Q., Bu, X., Long, Z. and Xu, Y. (1995), "Generalized conforming plate bending elements using point and line compatibility conditions", *Comput. Struct.*, **54**(4), 717-723.
- Long, Y.Q. and Xin, K. (1989), "Generalized conforming element for bending and buckling analysis of plates", *Finite Elements in Analysis and Design*, **5**, 15-30.
- Long, Y.Q. and Xu, Y. (1994), "Generalized conforming triangular membrane element with rigid rotational freedoms", *Finite Elements in Analysis and Design*, **17**, 259-271.
- Long, Y.Q. and Zhao, J. (1988), "A new generalized conforming triangular element for thin plates", *Communications in Applied Numerical Methods*, **4**, 781-792.
- Long, Z.F. (1992), "Triangular and rectangular plate elements based on generalized compatibility conditions", *Comput. Mech.*, **10**, 281-288.
- Long, Z.F. (1993), "Two generalized conforming plate elements based on semiLoof constrains", *Comput. Struct.*, **47**(2), 299-304.
- Morley, L.S.D. (1963), *Skew Plates and Structures*, International Series of Monographs in Aeronautics and Astronautics, Macmillan, New York.
- Olson, M.D. and Bearden, T.W. (1979), "The simple flat triangular shell element revisited", *Int. J. Numer. Meth. Eng.*, **14**, 51-68.
- Parisch, H. (1979), "A critical survey of the 9-node degenerated shell element with special emphasis on thin shell", *Comput. Method Appl. Mech. Eng.*, **20**, 323-350.
- Providas, E. and Kattis, M.A. (2000), "An assessment of two fundamental flat triangular shell elements with drilling rotations", *Comput. Struct.*, **77**(2), 129-139.
- Razzaque, A. (1973), "Program for triangular bending elements with derivative smoothing", *Int. J. Numer. Meth. Eng.*, **6**, 333-345.
- Saleeb, A.F., Chang, T.Y., Graf, W. and Yingyeunyong, S. (1990), "A hybrid/mixed model for non-linear shell analysis and its applications to large rotation problems", *Int. J. Numer. Meth. Eng.*, **29**, 407-446.
- Soh, A.K., Cen, S., Long, Y.Q. and Long, Z.F. (2001), "A new twelve DOF quadrilateral element for analysis of thick and thin plate", *European Journal of Mechanics A/Solids*, **20**(2), 299-326.
- Soh, A.K., Long, Z.F. and Cen, S. (1999), "A new nine DOF triangular element for analysis of thick and thin plates", *Comput. Mech.*, **24**, 408-417.
- Taylor, R.L. and Auricchio, F. (1993), "Linked interpolation for Reissner-Mindlin plate element: part II-a simple triangle", *Int. J. Numer. Meth. Eng.*, **36**, 3057-3066.
- To, C.W.S. and Liu, M.L. (1994), "Hybrid strain based three-node flat triangular shell elements", *Finite Elements in Analysis and Design*, **17**, 169-203.
- To, C.W.S. and Liu, M.L. (1995), "Hybrid strain based three-node flat triangular shell elements-II. Numerical investigation of nonlinear problems", *Comput. Struct.*, **54**(6), 1057-1076.
- Wanji, C. and Cheung, Y.K. (1998), "Refined triangular discrete Kirchhoff thin plate bending element", *Int. J. Numer. Meth. Eng.*, **41**, 1507-1525.
- Wanji, C. and Cheung, Y.K. (1999), "Refined non-conforming triangular elements for analysis of shell

- structures”, *Int. J. Numer. Meth. Eng.*, **46**, 433-455.
- Wanji, C. and Cheung, Y.K. (2001), “Refined 9-Dof triangular Mindlin plate elements”, *Int. J. Numer. Meth. Eng.*, **51**, 1259-1281.
- Zhang, Q., Lu, M. and Kuang, W. (1998), “Geometric non-linear analysis of space shell structures using generalized conforming flat shell elements for space shell structures”, *Communications in Numerical Methods in Engineering*, **14**, 941-957.
- Zhang, Y., Cheung, Y.K. and Chen, W.J. (2000), “Two refined nonconforming flat shell elements”, *Int. J. Numer. Meth. Eng.*, **49**, 355-382.
- Zienkiewicz, O.C. and Taylor, R.L. (2000), *The Finite Element Method (fifths edition), Volume 2: Solid Mechanics*, Butterworth-Heinemann, Oxford.
- Zienkiewicz, O.C., Xu, Z., Ling, F.Z., Samuelsson, A. and Wiberg, N.E. (1993), “Linked interpolation for Reissner-Mindlin plate element: part I-a simple quadrilateral”, *Int. J. Numer. Meth. Eng.*, **36**, 3043-3056.